

# Physisorption kinetics of electrons at plasma boundaries

F. X. Bronold, H. Deutsch, and H. Fehske

Institut für Physik, Ernst-Moritz-Arndt-Universität Greifswald, D-17489 Greifswald, Germany

Received: date / Revised version: date

**Abstract.** Plasma-boundaries floating in an ionized gas are usually negatively charged. They accumulate electrons more efficiently than ions which leads to the formation of a quasi-stationary electron film at the boundaries. We propose a physisorption-inspired quantum-kinetic description of the build-up of surface charges at inert plasma boundaries, where other surface modifications, in particular, implantation of particles, reconstruction or destruction of the surface due to high energy particles, etc. do not occur. The electron sticking coefficient  $s_e$  and the electron desorption time  $\tau_e$ , which play an important role in determining the quasi-stationary surface charge, and about which little is empirically and theoretically known, can then be calculated from a relatively well-defined microscopic model for the electron-wall interaction. Within this approach, it turns out that the polarization-induced short-range part of the electron-wall interaction determines the binding energy of the electron, whereas the inelastic processes at the wall determine  $s_e$  and  $\tau_e$ . In particular the inelastic channels depend strongly on the material. As an example we specifically discuss a metallic boundary. Assuming the plasma electron to loose (gain) energy at the surface by creating (annihilating) electron-hole pairs in the metal, we find  $s_e \approx 10^{-4}$  and  $\tau_e \approx 10^{-2}$  s. The product  $s_e \tau_e \approx 10^{-6}$  s has the order of magnitude expected from our earlier results for the charge of dust particles in a plasma but individually  $s_e$  is unexpectedly small and  $\tau_e$  is unexpectedly large. However, since the binding energy of the electron turns out to be much larger than  $kT_s$ , where  $T_s$  is the wall temperature, this, at first sight perhaps unexpected result, can be understood. Nevertheless, further investigations, both theoretical and experimental, are clearly needed. If  $s_e$  is indeed as small as our exploratory calculation suggests, it would have severe consequences for the way the formation of surface charges should be described. To identify what we believe are key issues of the electronic microphysics at inert plasma boundaries and to inspire other groups to join us on our journey is the purpose of this colloquial presentation.

**PACS.** 52.27.Lw Dusty or complex plasmas – 52.40.Hf Plasma-material interaction, boundary layer effects – 68.43.-h Chemi-/Physisorption: adsorbates on surfaces – 73.20.-r Electron states at surfaces and interfaces

## 1 Introduction

Low-temperature plasma physics is undoubtedly an applied science driven by the ever increasing demand for plasma-assisted surface modification processes and environmentally save, low-power consuming lighting devices. At the same time, however, the physics of gas discharges is rich on fundamental problems which are of broader interest.

From a formal point of view, a gas discharge is an externally driven bounded reactive multicomponent system. It contains, besides electrons and positive ions, chemically reactive atoms or molecules strongly interacting with each other and with internal ( $nm$  to  $\mu m$ -sized solid particles) and external (walls of the discharge vessel) boundaries. Like in any reactive system elementary collision processes (elastic, inelastic, and reactive), occurring on a microscopic scale, determine in conjunction with external control parameters the global properties of the system on the macroscopic scale. For a gas discharge there are at least two macroscopic scales: the electromagnetic scale,

where screening and sheath formation takes place [1,2], and the spatial extension of the whole discharge. The physical properties of gas discharges are thus the manifestations of a subtle interplay of processes occurring on at least three different scales. Being externally driven, low-temperature plasmas are in addition usually far-off thermal equilibrium and like other dissipative systems feature a great variety of self-organization phenomena [3,4]. Finally, and this sets the theme of this colloquium, low-temperature gas discharges, in contrast to magnetically confined high-temperature fusion plasmas, are bounded by macroscopic objects. Thus, they strongly interact with solids.

The plasma-solid interaction is of course at the core of all plasma-assisted surface processes (deposition, implantation, sputtering, etching, etc.) [5]. Of more fundamental interest, however, is the situation of a chemically inert (i.e., no surface modification due to chemical processes, no reconstruction or destruction of the surface due to high-energy particles etc.) floating surface, where the interaction with the plasma leads only to the build-up of

surface charges and thus to a quasi-two-dimensional electron film which may have universal properties similar to electrons trapped on a liquid helium surface [6] or to electrons confined at a semiconductor heterojunction [7].

In plasma-physical settings surface charges play a role in atmospheric plasmas, where the charge of  $nm$ -sized aerosols [8] is of interest, in space bound plasmas, where surface charges of space crafts [9, 10] and of interplanetary and interstellar dust particles [11, 12] have been extensively studied, and in laboratory dusty plasmas, where the study of self-organization of highly negatively charged, strongly interacting  $\mu m$ -sized dust particles became an extremely active area of current plasma research [13, 14, 15, 16, 17, 18, 19]. Recently, surface charges affecting the physics of dielectric barrier discharges attracted also a lot of attention [20, 21, 22, 23, 24, 25].

That surface charges at plasma boundaries could be considered as a thin film of adsorbed electrons (“surface plasma”) in contact with the bulk plasma was originally suggested by Emeleus and Coulter in one of their investigations of wall recombination in the positive column [26]. Later, Behnke and coworkers [27] used this idea to phenomenologically construct boundary conditions for the kinetic equations describing glow discharges and Kersten *et al.* [28] employed the notation of a surface plasma to study the charging of dust particles in a plasma.

Although the surface plasma as a physical entity with its own physical properties is implicitly contained in these investigations, a microscopic description of its formation, dynamics, and structure was not attempted. First steps in this direction were taken by us in a short note [29]. The purpose of this colloquium is to extend these considerations and to convey the conviction that the concept of a surface plasma is not empty. On the contrary, it enables one to ask fundamental questions about plasma-wall interaction which are of broader interest. To list just a few:

- What forces bind electrons and ions to the plasma boundary?
- How do electrons and ions dissipate energy when approaching the boundary?
- What is the probability with which an electron sticks at or desorbs from the boundary?
- What is the density and temperature of the surface plasma and are there any collective properties?
- What is the mobility for the lateral motion of electrons and ions along the wall and can it be controlled by external electromagnetic fields?
- How does all this affect electron-ion recombination and secondary electron emission on chemically inert plasma boundaries?

The microphysics responsible for the formation of a surface plasma at an inert plasma boundary is schematically shown in Fig 1. Electrons and ions are collected from the plasma with collection fluxes  $j_{e,i}^{\text{coll}} = s_{e,i} j_{e,i}^{\text{plasma}}$ , where  $s_{e,i}$  are the sticking coefficients and  $j_{e,i}^{\text{plasma}}$  are the fluxes of plasma electrons and ions hitting the boundary. Electrons and ions may thermally desorb from the boundary with rates  $\tau_{e,i}^{-1}$ , where  $\tau_{e,i}$  are the desorption times. They may

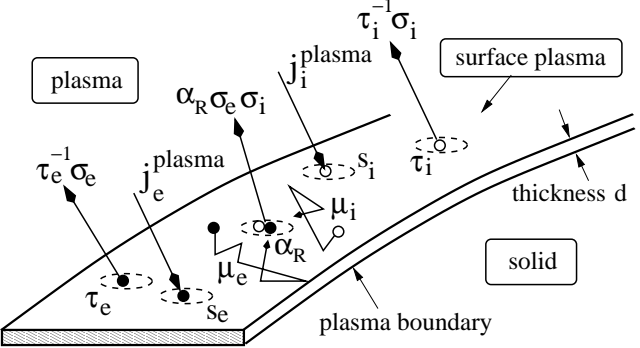


**Fig. 1.** Illustration of the elementary surface processes leading to the build-up of a quasi-stationary surface plasma at an inert plasma boundary.

also move along the surface with mobilities  $\mu_{e,i}$ , which in turn may affect the probability  $\alpha_R$  with which ions recombine with electrons at the wall. All these processes occur in a layer whose thickness  $d$  is at most a few microns, that is, on a scale where the standard kinetic description of the gas discharge based on the Boltzmann-Poisson system breaks down. Thus, the above listed questions can be only addressed from a quantum-mechanical point of view.

Of particular importance for the quantitative description of the build-up of a surface plasma are the sticking coefficients  $s_{e,i}$  and the desorption times  $\tau_{e,i}$ . Little is quantitatively known about these parameters, in particular, with respect to the electrons. Very often,  $s_e \approx s_i \approx 0.1 - 1$  and  $\tau_e^{-1} = \tau_i^{-1} = 0$  is used without further justification. Below, we develop a quantum-kinetic approach to calculate  $s_e$  and  $\tau_e$  from a microscopic model for the plasma boundary interaction. For that purpose, we treat the interaction of electrons with plasma boundaries as a physisorption process [30, 31, 32, 33, 34, 35, 36, 37, 38, 39] in the polarization-induced attractive part of the surface potential. Electron surface states [40, 41, 42, 43, 44, 45, 46, 47, 48, 49, 50, 51], a few  $nm$  away from the boundary, will thus play a central role as will surface-bound scattering processes which control electron energy relaxation at the surface and thus electron sticking and desorption.

Although the forces and scales are different for ions, they behave, from our point of view, conceptually very similar. The main difference between electrons and ions is that as soon as the surface collected some electrons, because of the faster bombardment with electrons than with ions, the surface potential for ions is the attractive Coulomb potential (most probably screened but that's for the following irrelevant). Hence, the ion surface states are deep in the sheath and thus, on a microscopic scale, far away from the surface. The microscopic processes driving ion energy relaxation and eventually ion sticking and desorption are thus not surface- but plasma-bound.

In the microscopic theory presented below, we want to exclusively focus on the physics occurring at most a few  $nm$  away from the boundary. We will therefore not give here a quantitative treatment of the physisorption kinetics of ions. However, when it comes to the construction of constituting equations for the surface charge, we have

to make some assumptions about the ion dynamics and kinetics. We will then discuss ions at least qualitatively. The assumptions made for ions, which are somewhat in conflict with what other people expect [52, 53, 54], do not affect the microscopic calculation of  $s_e$  and  $\tau_e$ .

The outline of this colloquium is then as follows. In the next section we describe and put into context the surface model for the charge of a floating dust particle in a plasma we developed in [29] because it motivated the physisorption-inspired microscopic treatment of electrons at plasma boundaries discussed in this colloquium. A qualitative description of the ion kinetics in the vicinity of a spherical grain is also included in this section. The following two sections will be however only concerned with electrons. Section 3 describes a microscopic model for the interaction of electrons with plasma boundaries. Specified to a metallic boundary, it will then be used to calculate the electron sticking coefficient  $s_e$  and the electron desorption time  $\tau_e$ . Key issues of the microscopic description of the electron-wall interaction (surface potential, coupling to elementary excitations of the solid, etc.) will be identified and numerical results will be presented and discussed. A critique of our assumptions and a list of to-do's is given in section 4 before we close the presentation in section 5 with a few concluding remarks. Mathematical details which may interrupt the flow of the presentation are relegated to two appendices.

## 2 Charge of a dust particle in a plasma

The physisorption-inspired treatment of surface charges originated from our attempt to calculate the charge of a spherical  $\mu\text{m}$ -sized floating dust particle in a plasma, taking not only plasma-induced but also surface-induced processes into account [29]. Here we have to clearly distinguish between the assumptions made to construct a condition from which the surface charge is determined and the assumptions made to obtain estimates for the electron surface parameters required in our model. As mentioned in the introduction, the hypotheses we make about the ion dynamics and kinetics affect only the former but are irrelevant for the calculation of the electronic surface parameters presented in the next sections.

### 2.1 Rate equations

First, we will discuss the surface model proposed in [29] from the perspective of the rate equations corresponding to the elementary processes shown in Fig. 1. Thereby we also identify the assumptions, in particular, with respect to the surface properties, which are usually made in standard calculations of surface charges.

To be specific let us consider a spherical dust particle with radius  $R$ . The quasi-stationary charge of the grain is given by (we measure charge in units of  $-e$ )

$$Z_p = 4\pi R^2 [\sigma_e - \sigma_i] , \quad (1)$$

with electron and ion surface densities,  $\sigma_{e,i}$ , satisfying the quasi-stationary ( $d\sigma_{e,i}/dt = 0$ ) rate equations [28],

$$0 = s_e j_e^{\text{plasma}} - \tau_e^{-1} \sigma_e - \alpha_R \sigma_e \sigma_i , \quad (2)$$

$$0 = s_i j_i^{\text{plasma}} - \tau_i^{-1} \sigma_i - \alpha_R \sigma_e \sigma_i , \quad (3)$$

where  $j_{e,i}^{\text{plasma}}$ ,  $s_{e,i}$ ,  $\tau_{e,i}$ , and  $\alpha_R$  denote, respectively, the fluxes of electrons and ions hitting the grain surface from the plasma, the electron and ion sticking coefficients, the electron and ion desorption times, and the electron-ion recombination coefficient.

In order to derive the standard criterion invoked to determine the quasi-stationary grain charge, we now assume, in contrast to what we do in our model [29] (see also below), that both electrons and ions reach the surface of the grain. In that case, both Eq. (2) and Eq. (3) should be interpreted as flux balances on the grain surface. At quasi-stationarity, the grain is charged to the floating potential. In energy units  $\bar{U} = Z_p e^2 / R$ . Because the grain temperature  $kT_s \ll \bar{U}$  the ion desorption rate  $\tau_i^{-1} \approx 0$ . Equation (3) reduces therefore to  $\alpha_R \sigma_e \sigma_i = s_i j_i^{\text{plasma}}$  which transforms Eq. (2) into  $s_e j_e^{\text{plasma}} = s_i j_i^{\text{plasma}} + \tau_e^{-1} \sigma$  provided  $\sigma \approx \sigma_e$  which is usually the case. In the standard approach the grain surface is assumed to be a perfect absorber for electrons and ions. Thus,  $s_i = s_e = 1$  and  $\tau_e^{-1} = 0$ . The quasi-stationary charge  $Z_p$  of the grain is then obtained from the condition

$$j_e^{\text{plasma}}(Z_p) = j_i^{\text{plasma}}(Z_p) , \quad (4)$$

where we explicitly indicated the dependence of the plasma fluxes on the grain charge.

Calculations of the grain charge differ primarily in the approximations made for the plasma fluxes  $j_{e,i}^{\text{plasma}}$ . For the repelled species, usually collisionless electrons, the flux can be obtained from Poisson's equation and the collisionless Boltzmann equation, using trajectory tracing techniques based on Liouville's theorem and momentum conservation [55, 56, 57]. The flux for the attracted species, usually collisional ions, is much harder to obtain. Unlike the electron flux, the ion flux depends not only on the field of the macroscopic body but also on scattering processes due to the surrounding plasma, which throughout we assume to be quiescent. For weak ion collisionalities the charge-exchange enhanced ion flux model proposed by Lampe and coworkers [52, 53, 54] is usually used although its validity has been questioned by Tskhakaya and coworkers [58, 59]. We come back to Lampe and coworkers approach below when we discuss representative results for our surface model.

Irrespective of the approximations made for the plasma fluxes, the standard approach of calculating surface charges is based on three assumptions about the surface physics:

- Ions and electrons reach the surface, even on the microscopic scale.
- $s_e = s_i = 1$  or at least  $s_e = s_i$ .
- $\tau_e^{-1} = 0$  or at least  $\tau_e^{-1} \sigma_e \ll s_i j_i^{\text{plasma}} = \alpha_R \sigma_e \sigma_i$ .

We basically question all three assumptions.

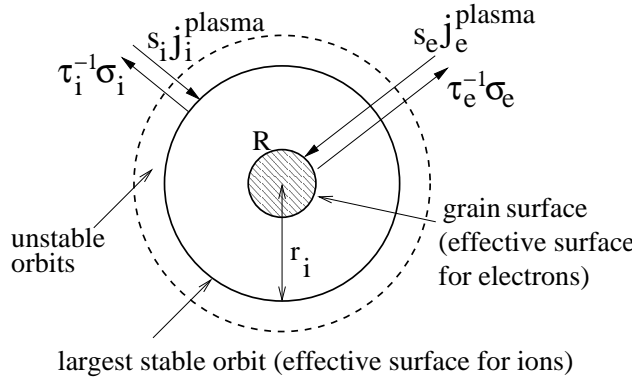


**Fig. 2.** Illustration of the surface model for the charging of a dust particle with radius  $R$  in a gas discharge. At quasi-stationarity, surface charges  $\sigma_{e,i}$  bound at  $r_e \approx R$  and  $r_i \gtrsim r_e$ , respectively, balance the collection flux  $s_{e,i} j_{e,i}^{\text{plasma}}$  with the respective desorption flux  $\tau_{e,i}^{-1} \sigma_{e,i}$ , where  $s_{e,i}$  and  $\tau_{e,i}$  denote, respectively, sticking coefficients and desorption times [29].

First, electrons and ions should be bound in external surface states. Because of differences in the potential energy and the mass, the spatial extension of the electron and ion bound states, and thus the distance of electrons and ions from the boundary, is expected to be different. On the microscopic scale, electrons and ions should be spatially separated.

Second,  $s_e = s_i$  is quite unlikely. Usually, heavy particles, such as ions, couple rather strongly to vibrational excitations of the boundary [35,38]. They can thus dissipate energy very efficiently which usually leads to a large sticking coefficient. Light particles, like electrons, on the other hand, couple only very weakly to vibrations of the boundary. On this basis, we would expect  $s_e \ll s_i$ . To what extend the coupling to other elementary excitations of the boundary (plasmons, electron-hole pairs, ...) can compensate for the lack of efficient coupling to lattice vibrations is part of our investigations.

Third, if ions and electrons are indeed spatially separated, the two rate equations should be interpreted as flux balances on two different effective surfaces (viz: the two closed circles in Fig. 2). In that case,  $\alpha_R \sigma_i \sigma_e \ll \sigma_{e,i}/\tau_{e,i}$  and the surface charge  $Z_p$  would be determined by balancing on the grain surface the electron desorption flux,  $\tau_e^{-1} \sigma_e$ , with the electron collection flux,  $s_{e,i} j_e^{\text{plasma}}$ . The corresponding balance of ion fluxes, to be taken on an effective surface surrounding the grain, would then yield a partial screening charge  $Z_i$ . Within this scenario, we would thus obtain

$$Z_p = 4\pi r_e^2 \cdot (s\tau)_e \cdot j_e^{\text{plasma}}(Z_p), \quad (5)$$

$$Z_i = 4\pi r_i^2 \cdot (s\tau)_i \cdot j_i^{\text{plasma}}, \quad (6)$$

with  $r_e \approx R$  and  $r_i \gtrsim r_e$ .

The surface physics is encoded in  $(s\tau)_{e,i}$ . These products depend on the material and on the plasma. They could be used as adjustable parameters. A justification of the assumptions, however, made in deriving Eqs. (5) and (6) can only come from a microscopic calculation of

$(s\tau)_{e,i}$ . For electrons this will be done in the following sections.

## 2.2 Semi-microscopic approach

Before we describe the microscopic calculation of  $s_e$  and  $\tau_e$  we summarize, to prepare the grounds for a microscopic thinking and to demonstrate that Eqs. (5) and (6) give results which compare favorable with experimental data, the semi-microscopic approach taken in Ref. [29].

It is based on a quantum mechanical investigation of the bound states of a negatively charged particle in a gas discharge. More specifically, we considered the static interaction between an electron (ion) with charge  $-e$  ( $+e$ ) and a spherical particle with radius  $R$ , dielectric constant  $\epsilon$ , and charge  $Z_p$ . The interaction potential contains a polarization-induced part, arising from the electric boundary conditions at the grain surface, and a Coulomb tail due to the particle's charge [60,61].

By now a few remarks about the Coulomb part of the potential are in order. The polarization part will be discussed at greater length in the next section. Microscopically, the Coulomb part arises from the interaction between the approaching electron and the electrons already residing on the grain. From electrons attached to a liquid helium film it is known that this interaction can be rather involved, in particular, when the electrons comprising the film are allowed to respond dynamically [62]. Below we assume the electrons on the grain (and implicitly also on planar surfaces) to be smeared out and approximate the Coulomb part by the potential of a sphere (plane) with charge  $Z_p$ . This is equivalent to treat the individual electron-electron interactions in a meanfield approximation, neglecting dynamical effects due to the polarization of the electron film.

Measuring distances from the grain surface in units of  $R$  and energies in units of  $\bar{U}$ , the interaction energy at  $x = r/R - 1 > x_b$ , where  $x_b$  is a lower cut-off, below which the grain boundary cannot be described as a perfect surface anymore, reads

$$V_{e,i}(x) = \pm \frac{1}{1+x} - \frac{\xi}{x(1+x)^2(2+x)} \approx \begin{cases} 1 - \xi/2x & \text{electron} \\ -1/(1+x) & \text{ion} \end{cases} \quad (7)$$

with  $\xi = (\epsilon - 1)/2(\epsilon + 1)Z_p$ .

The second line in Eq. (7) is an approximation which describes the relevant parts of the potential very well and permits an analytical calculation of the surface states. In Fig. 3 we plot  $V_{e,i}(x)$  for a melamine-formaldehyde (MF) particle ( $\epsilon = 8$ ,  $R = 1 \mu\text{m}$ , and  $Z_p = 1500$ ) embedded in a  $100\text{Pa}$  neon discharge with plasma density  $n_e = n_i = 0.39 \times 10^9 \text{ cm}^{-3}$ , ion temperature  $k_B T_i = 0.026 \text{ eV}$ , and electron temperature  $k_B T_e = 6.3 \text{ eV}$  [15]. From the electron energy distribution,  $f_e(E)$ , we see that the discharge contains enough electrons which can overcome the Coulomb barrier of the particle. These electrons may get bound in the polarization-induced short-range part of the

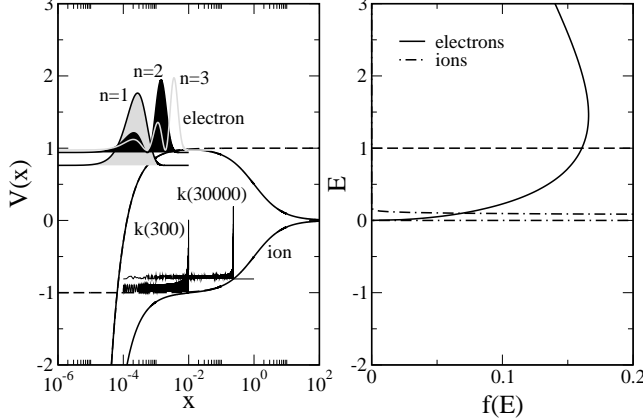


**Fig. 3.** Left panel: Potential energy for an electron (ion) in the field of a MF particle ( $R = 1 \mu\text{m}$ ,  $Z = 1500$ ) [15] and representative probability distributions,  $|u(x)|^2$ , shifted to the binding energy and maxima normalized to one. Dashed lines denote the potentials used in the Schrödinger equations. Note, the finite ion radius  $r_i^{\text{size}} \sim \text{\AA}$  forces the ion wavefunctions to vanish at  $x \approx 10^{-4}$ . Right panel: Bulk energy distribution functions for the  $100\text{Pa}$  neon discharge hosting the particle [15]:  $kT_e = 6.3\text{ eV}$ ,  $kT_i = 0.026\text{ eV}$ , and  $n_e = n_i = 0.39 \times 10^9 \text{ cm}^{-3}$ .

potential, well described by the approximate expression, provided they can get rid of their kinetic energy. Ions, on the other hand, being cold (see  $f_i(E)$  in Fig. 3) and having a finite radius  $r_i^{\text{size}}/R = x_i^{\text{size}} \gtrsim 10^{-4}$ , cannot explore the potential at short distances. For them, the long-range Coulomb tail is most relevant, which is again well described by the approximate expression.

Writing for the electron eigenvalue  $\varepsilon^e = 1 - \alpha_e \xi / 4k^2$  with  $\alpha_e = (\epsilon - 1)R/4(\epsilon + 1)a_B$  and for the ion eigenvalue  $\varepsilon^i = -\alpha_i/2k^2$  with  $\alpha_i = m_i R Z_p / m_e a_B$ , where  $a_B$  is the Bohr radius and  $m_e$  and  $m_i$  are the electron and ion mass, respectively, the radial Schrödinger equations for the approximate potentials read

$$\frac{d^2 u^{e,i}}{dx^2} + \left[ -\frac{\alpha_{e,i}^2}{k^2} + \tilde{V}_{e,i}(x) - \frac{l(l+1)}{(1+x)^2} \right] u^{e,i} = 0 \quad (8)$$

with  $\tilde{V}_e(x) = 2\alpha_e/x$  and  $\tilde{V}_i(x) = 2\alpha_i/(1+x)$ . For bound states, the wavefunctions have to vanish for  $x \rightarrow \infty$ . The boundary condition at  $x_b$  depends on the potential for  $x \leq x_b$ , that is, on the surface barrier (which is different for electrons and ions). Matching the solutions for  $x < x_b$  and  $x > x_b$  at  $x = x_b$  leads to a secular equation for  $k$ . For our purpose, it is sufficient to take the simplest model for the barrier:  $\tilde{V}_{e,i}(x \leq x_b) = \infty$  with  $x_b = 0$  for electrons and  $x_b = x_i^{\text{size}}$  for ions.

The electron Schrödinger equation is then equivalent to the Schrödinger equation for the hydrogen atom and  $k$  is an integer  $n$ . Because (for bound electrons)  $x \ll 1$  and  $\alpha_e \gg 1$ , the centrifugal term is negligible. Hence, we consider only states with  $l = 0$ . The eigenvalues are then

$\varepsilon_n^e = 1 - \alpha_e \xi / 4n^2$  and the wavefunctions read

$$u_{n,0}^e(x) \sim v_{n,0}(\bar{z}) \\ = \bar{z} \exp(-\bar{z}/2) (-)^{n-1} (n-1)! L_{n-1}^{(1)}(\bar{z}) \quad (9)$$

with  $\bar{z} = 2\alpha_e x / n$  and  $L_n^{(1)}(\bar{z})$  associated Laguerre polynomials.

The probability densities  $|u_{n,0}^e(x)|^2$  for the first three states are plotted in Fig. 3. As can be seen, electron surface states are only a few Ångstroms away from the grain boundary. At these distances, the spatial variation of  $V_e(x)$  is comparable to the de-Broglie wavelength of electrons approaching the particle. More specifically, for  $k_B T_e = 6.3\text{ eV}$ ,  $\lambda_e^{dB}/R \approx |V_e/V'_e| \approx 10^{-4}$ . Hence, the trapping of electrons at the surface of the particle has to be described quantum-mechanically.

The solutions of the ion Schrödinger equation are Whittaker functions,  $u_{k,l}^i(x) = W_{k,l+1/2}(\bar{x})$  with  $\bar{x} = 2\alpha_i(1+x)/k$  and  $k$  determined from  $u_{k,l}^i(x_i^{\text{size}}) = 0$ . However, since  $k \gg 1$  and  $\bar{x} \gg 1$ , it is very hard to work directly with  $W_{k,l+1/2}(\bar{x})$ . It is easier to use the method of comparison equations [63] and to construct uniform approximations for  $u_{k,l}^i(x)$  with the radial Schrödinger equation for the hydrogen atom as a comparison equation. The method can be applied for any  $l$ . Here we give only the result for  $l = 0$ :

$$u_{k,0}^i(x) \sim v_{n,0}(\bar{z}) / \sqrt{dz/dx} \quad (10)$$

with  $v_{n,0}(\bar{z})$  defined in Eq. (9) and  $\bar{z} = 2\alpha_i z(x)/n$ . The mappings  $z(x)$  and  $k(n)$  can be constructed from the phase-integrals of the two Schrödinger equations.

In Fig. 3 we show  $|u_{k,0}^i(x)|^2$  for  $k(300)$  and  $k(30000)$ . Note, even the  $k(30000)$  state is basically at the bottom of the potential. This is a consequence of  $\alpha_i \gg 1$  which leads to a continuum of states below the ion ionization threshold at  $\varepsilon = 0$ . We also note that  $|u_{k(n),0}^i(x)|^2$  peaks for  $n \gg 1$  just below the turning point. Hence, except for the lowest states, which we expect to be of little importance, ions are essentially trapped in classical orbits deep in the sheath of the grain. This will be also the case for  $l > 0$ . That ions behave classically is not unexpected because for  $k_B T_i = 0.026\text{ eV}$  their de-Broglie wavelength is much smaller than the scale on which the potential varies for  $x > 10^{-3}$ :  $\lambda_i^{dB}/R \sim 10^{-5} \ll |V_i/V'_i| \sim 1$ . Thus, the interaction between ions and the particle is classical.

Nevertheless it is possible to describe ions quantum-mechanically. We anticipate the method of comparison equations, which is an asymptotic technique, to be rather useful in this respect. Since the ion dynamics and kinetics is beyond the scope of this paper, we do not give more mathematical details concerning the solution of the ion Schrödinger equation. We mention however that many years ago Liu [64] pursued a quantum-mechanical description of the collisionless ion dynamics around electric probes. But he found no followers.

A model for the charge of the grain which takes surface states into account can now be constructed as follows. Within the sheath of the particle, the density of

free electrons (ions) is much smaller than the density of bound electrons (ions). In that region, the quasi-stationary charge (again in units of  $-e$ ) is thus approximately given by

$$Z(x) = 4\pi R^3 \int_{x_b}^x dx' (1+x')^2 \left[ n_e^b(x') - n_i^b(x') \right] \quad (11)$$

with  $x < \lambda_i^D = \sqrt{4\pi k T_i / e n_i}$ , the ion Debye length, which we take as an upper cut-off, and  $n_{e,i}^b$  the density of bound electrons and ions. For the plasma parameters used in Fig. 3,  $\lambda_i^D \approx 60\mu\text{m}$ . The results for the surface states presented above suggest to express the density of bound electrons by an electron surface density:

$$n_e^b(x) \approx \sigma_e \delta(x - x_e) / R \quad (12)$$

with  $x_e \approx x_b \approx 0$  and  $\sigma_e$  the quasi-stationary solution of Eq. (2) without the recombination term. Eq. (2) is thus still interpreted as a rate equation on the grain surface. We will argue below that once the grain has collected some negative charge, not necessarily the quasi-stationary one, there is a critical ion orbit at  $x_i \sim 1 - 10 \gg x_e$  which prevents ions from hitting the particle surface. Thus, the particle charge obtained from Eq. (11) is simply  $Z_p \equiv Z(x_e < x < x_i)$ . Inserting Eq. (12) into Eq. (11) and integrating up to  $x$  with  $x_e < x < x_i$  leads to Eq. (5), the expression for the particle charge deduced from the rate equations (2) and (3) under the assumption that ions do not reach the grain surface on the microscopic scale.

For an electron to get stuck at (to desorb from) a surface it has to loose (gain) energy at (from) the surface [35]. This can only occur through inelastic scattering with the grain surface. To calculate the product  $(\sigma\tau)_e$  requires therefore a microscopic description of energy relaxation at the grain surface. This will be done in the next section. In Ref. [29] we invoked the phenomenology of reaction rate theory and approximated  $(\sigma\tau)_e$  by

$$(\sigma\tau)_e = \frac{h}{k_B T_s} \exp \left[ \frac{E_e^d}{k_B T_s} \right], \quad (13)$$

where  $h$  is Planck's constant,  $T_s$  is the surface temperature, and  $E_e^d$  is the electron desorption energy, that is, the binding energy of the surface state from which desorption most likely occurs [35]. The great virtue of this equation is that it relates a combination of kinetic coefficients, which depend on the details of the inelastic (dynamic) interaction, to an energy, which can be deduced from the static interaction alone. Kinetic considerations are thus reduced to a minimum. They are only required to identify the relevant temperature and the state from which desorption most probably occurs. In the next section we will derive Eq. (13) from a microscopic theory for the particular case of an electron interacting with a metal and discuss the assumptions for its validity.

Equation (5) is a self-consistency equation for  $Z_p$ . Combined with Eq. (13), and approximating the electron plasma flux  $j_e^{\text{plasma}}$  by the orbital motion limited flux,

$$j_e^{\text{OML}} = n_e \sqrt{k_B T_e / 2\pi m_e} \exp[-Z_p e^2 / R k_B T_e], \quad (14)$$

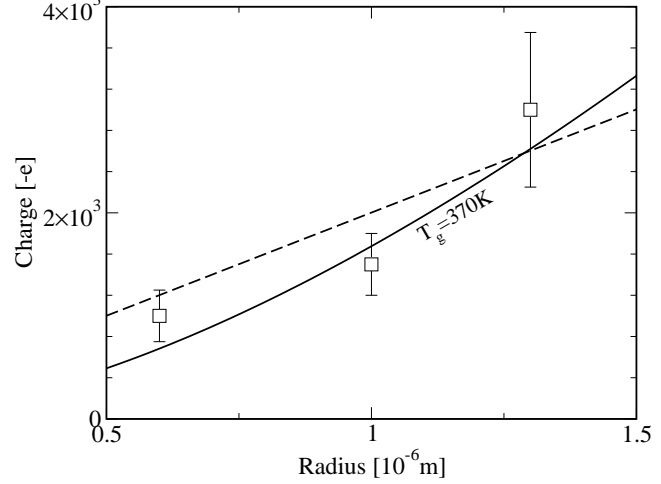


**Fig. 4.** Radius dependence of the charge of a MF particle in the bulk of a neon discharge at  $p = 100\text{Pa}$  [15]. The plasma parameters are the same as in Fig. 3. The solid line denotes the charges deduced from Eq. (15) and the dashed line gives the charges obtained from  $j_e^{\text{OML}} = j_i^{\text{OML}} + j_i^{\text{CX}}$  with  $\sigma_{\text{cx}} = 10^{-14}\text{cm}^{-2}$ .

which is reasonable, because, on the plasma scale, electrons are repelled from the grain surface, the grain charge is given by

$$Z_p = 4\pi R^2 \frac{h}{k_B T_s} e^{E_e^d / k_B T_s} j_e^{\text{OML}}(Z_p). \quad (15)$$

Thus, in addition to the plasma parameters  $n_e$  and  $T_e$ , the charge depends on the surface parameters  $T_s$  and  $E_e^d$ .

Without a microscopic theory for the inelastic electron-grain interaction, a plausible estimate for  $E_e^d$  has to be found from physical considerations alone. Since by necessity the electron comes very close to the grain surface (see Fig. 3) it will strongly couple to elementary excitations of the grain. Depending on the material these may be bulk or surface phonons, bulk or surface plasmons, or internal electron-hole pairs. For any realistic surface barrier, where the electron wavefunction leaks into the solid, the electron will therefore quickly relax to the lowest surface bound state. (The relaxation mechanism we discuss in the next section for a metal works also for an infinitely high barrier.) The  $n = 1$  state for the infinitely high barrier is an approximation to that state. Thus, it is reasonable to expect

$$E_e^d \approx (1 - \varepsilon_1^e) \bar{U} = \frac{R_0}{16} \left( \frac{\epsilon - 1}{\epsilon + 1} \right)^2, \quad (16)$$

which, for an MF particle with  $\epsilon = 8$ , leads to  $E_e^d \approx 0.5\text{eV}$ . The particle temperature cannot be determined in a simple way. It depends on the balance of heating and cooling fluxes to-and-fro the particle and thus on additional surface parameters [65]. We use  $T_s$  therefore as an adjustable parameter. To reproduce, for instance, with Eq. (15) the charge of the particle in Fig. 3,  $T_s = 370\text{ K}$  implying  $(\sigma\tau)_e \approx 10^{-6}\text{s}$ .

In Fig. 4 we plot the radius dependence of the charge of a MF particle in the  $100Pa$  neon discharge specified in the caption of Fig. 3. More results are given in [29]. Since the plasma parameters are known the only adjustable parameter is the surface temperature. Using  $T_s = 370K$  we find excellent agreement between theory and experiment. For comparison we also show the charges obtained from Eq. (4), approximating the ion plasma flux by

$$j_i^{\text{plasma}} = j_i^{\text{OML}} + j_i^{\text{cx}}, \quad (17)$$

where

$$j_i^{\text{OML}} = n_i \sqrt{k_B T_i / 2\pi m_i} [1 + Z_p e^2 / R k_B T_i] \quad (18)$$

is the orbital motion limited ion flux and [15]

$$j_i^{\text{cx}} = n_i (0.1 \lambda_i^D / l_{\text{cx}}) \sqrt{k_B T_i / 2\pi m_i} (Z_p e^2 / R k_B T_i)^2 \quad (19)$$

is the ion flux originating from the release of trapped ions due to charge-exchange scattering as suggested by Lampe and coworkers [52, 53, 54]. The scattering length  $l_{\text{cx}} = (\sigma_{\text{cx}} n_g)^{-1}$  with  $\sigma_{\text{cx}} = 10^{-14} \text{cm}^2$  the scattering cross section and  $n_g = p / k_B T_g$  the gas density. Clearly, the radius dependence of the grain charge seems to be closer to the nonlinear dependence obtained from Eq. (15) than to the linear dependence resulting from

$$j_e^{\text{OML}} = j_i^{\text{OML}} + j_i^{\text{cx}}, \quad (20)$$

indicating that the surface model we propose captures at least some of the physics responsible for the formation of surface charges.

In order to derive Eq. (15) from Eq. (11) we had to assume that once the particle is negatively charged ions are trapped far away from the grain surface. Treating trapping of ions in the field of the grain as a physisorption process suggests this assumption, which is perhaps counter-intuitive. Similar to an electron, an ion gets bound to the grain only when it loses energy. Because of its low energy and the long-range attractive ion-grain interaction, the ion will be initially bound very close to the ion ionization threshold (see Fig. 3). The coupling to the elementary excitations of the grain is thus negligible and only inelastic processes due to the plasma are able to push ions to lower bound states. Since the interaction is classical, inelastic collisions, for instance, charge-exchange scattering between ions and atoms, act like a random force. Ion energy relaxation can be thus envisaged as a de-stabilization of orbits. This is in accordance to what Lampe and coworkers assume [52, 53, 54]. In contrast to them, however, we [29] expect orbits whose spatial extension is smaller than the scattering length to be stable because the collision probability during one revolution becomes vanishingly small. For a circular orbit, a rough estimate for the critical radius is  $r_i = R(1 + x_i) = (2\pi\sigma_{\text{cx}} n_g)^{-1}$  which leads to  $x_i \sim 5.7 \gg x_e \sim 0$  when we use the parameters of the neon discharge of Fig. 3 and  $\sigma_{\text{cx}} = 10^{-14} \text{cm}^2$ .

Although the approach of Lampe *et al.* [52, 53, 54] shows a pile-up of trapped ions in a shell of a few  $\mu\text{m}$  radius

enclosing the grain, they would not expect a relaxation bottleneck. This point can be only clarified with a detailed investigation of the ion dynamics and kinetics in the vicinity of the grain. As mentioned before, despite the classical character of the ion dynamics, a quantum-mechanical treatment, similar to the one we will present in the following sections for electrons, is nevertheless possible and perhaps even advantageous because it treats closed (bound surface states) and open ion orbits (extended surface states) on the same footing. In addition, the existence of energy barriers due to the angular motion are easier to handle in a quantum mechanical context. In fact, Lampe and coworkers neglect these energy barriers whereas Tskhakaya and coworkers [58, 59] believe that this approximation overestimates  $j_i^{\text{cx}}$ . In reality, they claim,  $j_i^{\text{cx}}$  is much smaller. If this is indeed the case, the condition  $j_e^{\text{OML}} = j_i^{\text{OML}} + j_i^{\text{cx}}$  would yield charges which are much closer to the orbital-motion limited ones and thus far away from the experimentally measured charges.

Pushing the assumption of a critical ion orbit even further, we assumed in [29] that all trapped ions can be subsumed into a single effective orbit as shown in Fig. 2. We then obtained an intuitive expression for the number of ions accumulating in the vicinity of the grain, that is, for its partial screening charge. For that purpose we modelled the ion density  $n_i^b$  accumulating in the vicinity of the critical orbit by a surface density  $\sigma_i$  which balances at  $x_i$  the ion collection flux  $s_i j_i^{\text{plasma}}$  with the ion desorption flux  $\tau_i^{-1} \sigma_i$ . Mathematically, this gives rise to a rate equation similar to (3), with the recombination term neglected and interpreted as a rate equation at  $r = r_i$ . Although Eq. (13) assumes excitations of the grain to be responsible for sticking and desorption we expect a similar expression (with  $E_e^d$ ,  $T_s$  replaced by  $E_i^d$ ,  $T_g$ ) to control the density of trapped ions. Integrating (11) up to  $x$  with  $x_i < x < \lambda_i^D$  we then obtain  $Z(x_i < x < \lambda_i^D) = Z_p - Z_i$  with

$$Z_i = 4\pi R^2 (1 + x_i)^2 \frac{h}{k_B T_g} e^{E_i^d(Z_p) / k_B T_g} j_i^B \quad (21)$$

the number of trapped ions. Since the critical orbit is near the sheath-plasma boundary, it is fed by the Bohm ion flux  $j_i^B = 0.6 n_i \sqrt{k_B T_e / m_i}$ . The ion desorption energy is the negative of the binding energy of the critical orbit,  $E_i^d(Z_p) = -V_i(x_i) \bar{U}(Z_p) = 4\pi\sigma_{\text{cx}} a_B n_g Z_p R_0$ , and depends strongly on  $Z_p$  and  $x_i$ . For the situation shown in Fig. 3, we obtain  $E_i^d \approx 0.39 \text{eV}$  and  $(s\tau)_i \approx 10^{-8} \text{s}$  when we use  $T_g = T_s = 370 \text{K}$ , the particle temperature which reproduces  $Z_p \approx 1500$ . The ion screening charge is then  $Z_i \approx 12 \ll Z_p$  which is the order of magnitude expected from molecular dynamics simulations [66]. Thus, even when the particle charge is defined by  $Z(x_i < x < \lambda_i^D)$  it is basically given by  $Z_p$ .

From the surface model we would expect  $(s\tau)_e \sim 10^{-6} \text{s}$  to produce particle charges  $Z_p$  of the correct order of magnitude. Since the particle temperature  $T_s$  is unknown, it can be used as an adjustable parameter. The calculated  $Z_p$  can thus be always made to coincide with the measured charge. The particle temperature has to be of

course within physically meaningful bounds. Recently, the particle temperature (but unfortunately not the particle charge) has been measured [67]. There is thus some hope that in the near future  $Z_p$  and  $T_s$  will be simultaneously measured. Finally, let us point out that, because ions are in our model bound a few microns away from the surface, we obtain  $(s\tau)_i < (s\tau)_e$ , in agreement with the phenomenological fit performed in [28].

### 3 Physisorption of electrons

In the previous section we described a microscopic, physisorption-inspired model for the charging of a dust particle in a plasma which avoids the unrealistic treatment of the grain as a perfect absorber. Within this model the charge and partial screening of a dust particle can be calculated without relying on the condition that the total electron plasma flux balances on the grain surface the total ion plasma flux. Instead, two flux balance conditions are individually enforced on the two effective surfaces shown in Fig. 2 (solid circles). The quasi-stationary particle charge  $Z_p$  is then given by the number of electrons “quasi-bound” in the polarization potential of the grain and the screening charge  $Z_i$  is approximately given by the number of ions “quasi-trapped” in the largest stable closed ion orbit (which defines an effective surface for ions and subsumes, within our model, all trapped ions into a single effective orbit).

The microphysics at the grain boundary, in particular, the physisorption kinetics, that is, the sticking in and the desorption from external surface states due to inelastic scattering processes, is encoded in the products  $(s\tau)_{e,i}$  which we approximated by phenomenological expressions of the form (13). We now calculate  $s_e$  and  $\tau_e$  from a microscopic model for the electron-wall interaction, using a quantum-kinetic approach.

A similar calculation should be done for ions treating trapping and de-trapping of ions in the Coulomb potential as a physisorption process. However, the quantum-kinetic approach has then to be pushed to the semi-classical regime appropriate for ions, which significantly increases the mathematical complexity. Since moreover a plasma-based inelastic scattering process, most probably charge-exchange scattering, has to be invoked for ion energy relaxation, and not an inelastic processes involving the boundary itself, we consider a quantitative description of the physisorption kinetics of ions beyond the scope of the present paper.

#### 3.1 Interaction of electrons with plasma boundaries

The potential energy for an electron in the field of a negatively charged grain is a superposition of the Coulomb potential due to electrons already residing on the grain, which we treat in meanfield approximation (first term in Eq. (7)), and the polarization-induced image potential (second term in Eq. (7)).

As can be seen from Fig. 3, in the meanfield approximation, the long-range Coulomb repulsion leads only to a

barrier whose height is the floating energy  $\bar{U}$ . Only an electron with energy larger than  $\bar{U}$  has a chance to come close enough to the surface to feel the attractive polarization-induced short-range part of the potential. For an electron bound in this part of the potential, on the other hand, the Coulomb barrier merely sets the ionization threshold. Thus, as long as we treat the Coulomb repulsion in mean-field approximation, we can eliminate the Coulomb term from the considerations by simply measuring energies with respect to this threshold.

Let us now look at the distance from the surface where the polarization-induced attraction operates. It is very small. Even for  $\mu\text{m}$ -sized grains, the curvature of the surface can be neglected at these small distances. As far as the calculation of  $s_e$  and  $\tau_e$  is concerned, we can therefore, in a first approximation, consider a planar, uncharged surface.

A plasma electron approaching a planar, neutral boundary feels an attraction because of the polarization it induces on the surface of the solid. Putting the boundary in the  $xy$  plane and the plasma in the positive halfspace defined by  $z > 0$ , a convenient starting point for a microscopic description of the polarization-induced interaction between an electron and a boundary is the single electron Hamiltonian proposed by Evans and Mills [40],

$$H = -\frac{\hbar^2 \Delta}{2m_e} + \hbar\omega_s \sum_{\mathbf{K}} a_{\mathbf{K}}^\dagger a_{\mathbf{K}} + \sum_{\mathbf{K}} \Gamma(K) \exp[-i\mathbf{K} \cdot \mathbf{R} - Kz] (a_{\mathbf{K}}^\dagger + a_{-\mathbf{K}}) , \quad (22)$$

where  $\Delta$  is the three-dimensional Laplace operator,  $a_{\mathbf{K}}^\dagger$  is the creation operator for the polarization-induced surface mode responsible for the interaction, and

$$\Gamma(K) = \left( \frac{\pi e^2 \hbar \omega_s}{AK} \cdot \frac{\epsilon - 1}{\epsilon + 1} \right)^{\frac{1}{2}} \quad (23)$$

is the coupling function;  $\mathbf{K}$  is a two-dimensional wavevector,  $\mathbf{R} = (x, y)$  denotes the projection of the electron position onto the surface, whose area is  $A$ , and  $z$  is the distance of the electron from the surface. For metals ( $\epsilon = \infty$ ), the relevant surface modes are surface plasmons with typical energies of a few electron volts, for instance, for copper,  $\hbar\omega_s \approx 2\text{eV}$  [48]. For dielectrics ( $\epsilon < \infty$ ), on the other hand, the relevant surface modes are optical phonons with energies of a few tenth of an electron volt, for instance, for graphite,  $\hbar\omega_s \approx 0.43\text{eV}$  when we use  $\omega_s = \omega_T \sqrt{(\epsilon + 1)/2}$  with  $\epsilon = 12$  and  $\omega_T = 0.17\text{eV}$  [68].

To approximately separate the static from the dynamic interaction, we apply to the Hamiltonian (22) the unitary transformation [41],

$$U = \exp \left[ \sum_{\mathbf{K}} (\gamma_{\mathbf{K}}^*(\mathbf{R}, z) a_{\mathbf{K}}^\dagger - \gamma_{\mathbf{K}}(\mathbf{R}, z) a_{\mathbf{K}}) \right] , \quad (24)$$

with

$$\gamma_{\mathbf{K}}(\mathbf{R}, z) = \frac{\Gamma(K)}{\hbar\omega_s} \exp[i\mathbf{K} \cdot \mathbf{R} - Kz] \quad (25)$$

and obtain

$$\begin{aligned} \mathcal{H} &= UHU^\dagger \\ &= \sum_{\mathbf{Q}q} E_{\mathbf{Q}q} C_{\mathbf{Q}q}^\dagger C_{\mathbf{Q}q} + \hbar\omega_s \sum_{\mathbf{K}} a_{\mathbf{K}}^\dagger a_{\mathbf{K}} \\ &+ \sum_{\mathbf{Q}, \mathbf{K}} \sum_{q, q'} G_{qq'}(\mathbf{Q}, \mathbf{K})(a_{\mathbf{K}}^\dagger - a_{-\mathbf{K}}) C_{\mathbf{Q}-\mathbf{K}q}^\dagger C_{\mathbf{Q}q'} \quad (26) \end{aligned}$$

when we use the eigenstates of

$$\left( -\frac{\hbar^2}{2m_e} \Delta + V_p(z) \right) \Psi_{\mathbf{Q}q}(\mathbf{R}, z) = E_{\mathbf{Q}q} \Psi_{\mathbf{Q}q}(\mathbf{R}, z) \quad (27)$$

as a basis for the transformed Hamiltonian, that is, when  $C_{\mathbf{Q}q}^\dagger$  creates an electron in the surface state  $\Psi_{\mathbf{Q}q}$  with energy  $E_{\mathbf{Q}q}$ , where  $\mathbf{Q}$  is the two-dimensional wavevector characterizing the lateral motion of the electron and  $q$  is the quantum number for its vertical motion. For an unbound state  $q$  is a wavenumber  $k$  whereas for a bound state it is an integer  $n$ . As in the previous section, we assume an infinitely high surface barrier at  $z = 0$ . Thus,  $\Psi_{\mathbf{Q}q}(\mathbf{R}, z)$  vanishes at  $z = 0$  and is only defined for  $z \geq 0$ .

The static potential  $V_p(z)$  entering the Schrödinger equation (27) is given by

$$V_p(z) = - \sum_{\mathbf{Q}} \hbar\omega_s |\gamma_{\mathbf{Q}}(\mathbf{R}, z)|^2 = - \frac{e^2(\epsilon - 1)}{4(\epsilon + 1)z} \quad (28)$$

It is thus the classical image potential used in the previous section where the image plane coincides with the boundary. Hence,  $V_p(z)$  diverges at  $z = 0$ . The residual dynamical interaction encoded in the last term of Eq. (26) will in general modify this potential. In particular, it will shift the image plane. Strictly speaking, the classical image potential holds only at large enough distances, where the residual interaction becomes negligible and, as a result, the interaction between an electron and a surface is basically local and static.

Separating for the approaching electron the lateral from the vertical motion, the solutions of Eq. (27) can be written as

$$\Psi_{\mathbf{Q}q}(\mathbf{R}, z) = \frac{1}{\sqrt{A}} \exp[i\mathbf{Q} \cdot \mathbf{R}] \psi_q(z), \quad (29)$$

where  $\psi_q(z)$ , the electron wavefunction for the vertical motion, satisfies the one-dimensional Schrödinger equation (viz: Eq. (8)),

$$\frac{d^2}{dz^2} \psi_q(z) + \frac{2m_e}{\hbar^2} \left[ E_q - V_p(z) \right] \psi_q(z) = 0, \quad (30)$$

with  $E_q = E_{\mathbf{Q}q} - \hbar^2 Q^2 / 2m_e$  the energy in the vertical motion. The matrix element for the dynamic coupling between the electron and the surface becomes then

$$G_{qq'}(\mathbf{Q}, \mathbf{K}) = \frac{\hbar\Gamma(K)}{m\omega_s A} \left[ \mathbf{Q} \cdot \mathbf{K} J_{qq'}^{(1)}(K) - K J_{qq'}^{(2)}(K) \right] \quad (31)$$

**Table 1.** Dielectric constant  $\epsilon$ , Debye Energy  $kT_D$ , and the energy separations between the four lowest surface states for different materials.

material	$\epsilon$	$kT_D [eV]$	$\Delta E_{21} [eV]$	$\Delta E_{43} [eV]$
Cu	$\infty$	0.03	0.64	0.12
Si	12	0.057	0.46	0.09
graphite	12	0.19	0.46	0.09
$C_{60}$	4.5	0.016	0.26	0.05

with electronic matrix elements

$$J_{qq'}^{(1)}(K) = \int dz \psi_q^*(z) \exp[-Kz] \psi_{q'}(z), \quad (32)$$

$$J_{qq'}^{(2)}(K) = \int dz \psi_q^*(z) \exp[-Kz] \frac{d}{dz} \psi_{q'}(z). \quad (33)$$

In the long-wavelength approximation, that is, for  $K \rightarrow 0$ , the leading term of the matrix element is

$$G_{qq'}(\mathbf{Q}, \mathbf{K}) \approx \frac{\hbar\Gamma(K)}{m\omega_s A} \left[ \mathbf{Q} \cdot \mathbf{K} \delta_{qq'} - K J_{qq'}^{(2)}(0) \right]. \quad (34)$$

It thus contains intraband ( $q = q'$ ) and interband ( $q \neq q'$ ) transitions.

Sticking at and desorption from the surface clearly involves transitions between surface states with different vertical quantum numbers, that is, in the notation just introduced, interband transitions. Since the first term in Eq. (34) does not change the vertical quantum numbers, it does not contribute to sticking and desorption. Instead it primarily affects the mobility  $\mu_e$  of the electron along the surface (see Fig. 1). The second term in Eq. (34), on the other hand, could in principle give rise to sticking and desorption, in particular, when the energy of the surface mode is comparable to the surface temperature as well as to the energy spacing of the surface states due to  $V_p(z)$ . The approaching electron can then loose (gain) energy by creating (annihilating) real surface modes.

For dielectric boundaries, for instance, graphite, where  $\hbar\omega_s \approx 0.43eV \sim \Delta E_{21}$  (see table 1), the second term in Eq. (34) could thus be rather important. For metallic boundaries, however, the energy of the surface plasmon is  $\sim eV$  and thus far too high to play any role in the physisorption kinetics itself. In that case, only virtual interband transitions can be induced by the surface modes which leads to a renormalization of the eigenstates of the Schrödinger equation (27).

Technically, the renormalization of the eigenstates could be done perturbatively using diagrammatic techniques with the second term of Eq. (34) as a perturbation. Alternatively, following Ref. [40], the original Hamiltonian (22) could be also treated variationally. The renormalized static potential would then saturate at small distances. Hence, it would be finite at  $z = 0$ . The eigenstates of the corresponding Schrödinger equation, that is, the renormalized surface states, could be however only obtained numerically.

When the renormalization of the surface states due to the dynamic (interband) coupling to surface modes does

not destroy the spectrum of surface states, and there is plenty of experimental evidence for the existence of external surface states at various surfaces [42, 43, 44, 45, 46, 47, 48, 49, 50, 51], it is plausible to assume, in a first step, that the residual interaction (26) can be neglected and to consider the eigenstates of Eq. (27), or, when the lateral motion is separated away, the eigenfunctions of Eq. (30), as reasonable approximations for the true surface states.

A first estimate for the probability with which an electron approaching a plasma boundary ends up in a bound surface state (sticking), or with which an electron bound to a plasma boundary ends up in a free state (desorption) can thus be obtained from

$$\mathcal{H} = \sum_{Qq} E_{Qq} C_{Qq}^\dagger C_{Qq} + \mathcal{H}_s + \mathcal{H}_{es} , \quad (35)$$

where the first term describes the electron motion in the polarization-induced static surface potential, to be approximated by the classical image potential  $V_p(z)$ , the second term denotes the free motion of the low-energy elementary excitations of the boundary controlling energy relaxation and thus physisorption, and the third term is the coupling between the two.

Clearly, the specific form of (35) depends on the elementary excitations and hence on the material. For dielectric materials, such as graphite or silicon, electronic excitations, having at least the energy of the energy gap, that is, a few electron volts, can be safely neglected. It is the coupling to vibrational modes (possibly including the ones responsible for the polarization-induced surface states themselves, see discussion above) which most probably drives physisorption at dielectric surfaces. In particular, bulk vibrations, whose energy scale is the Debye energy  $kT_D$  are expected to play an important role. Notice, however, that the Debye energy of most dielectrics is smaller than the energy spacing of the two lowest surface states, even for graphite, whose Debye energy is rather high (see table 1). Multiphonon processes could thus significantly affect the physisorption of electrons on dielectric surfaces.

For metals, on the other hand, electronic excitations, most notably internal electron-hole pairs, are expected to play an important role [36, 39]. They are not created across a band gap but with respect to the Fermi energy of a partially filled band. They can thus be excited rather easily, even at room temperature. We expect therefore that for metallic plasma boundaries the coupling to internal electron-hole pairs controls the physisorption of plasma electrons.

We now specify the Hamiltonian (35) for the case of a metallic plasma boundary. An illustration of the microphysics at a metallic boundary is given in Fig. 5. The plasma occupies the halfspace for  $z > 0$  and the metal the halfspace for  $z < 0$ . (In the calculation we actually take two slaps with width  $L$ . We then let  $L$  go to infinity whereby it drops out from the final expression for  $s_e$  and  $\tau_e$  as does the area  $A$  of the boundary.) A transition between two external surface states is accompanied by the excitation or de-excitation of an electron-hole pair in the metal. Following [36, 39], we treat the metal as a free gas of

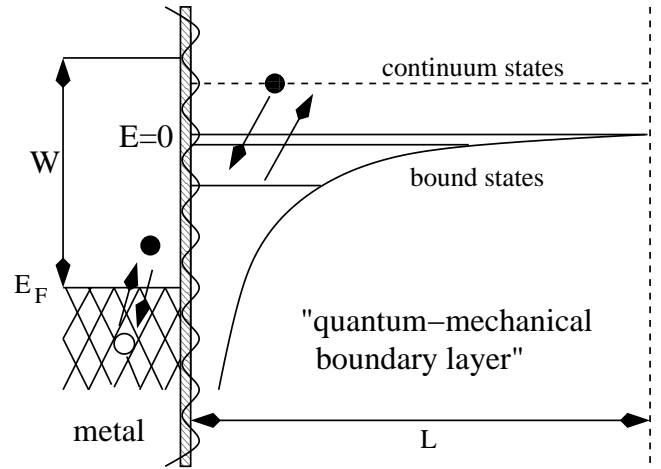


**Fig. 5.** Illustration of the microphysics for a plasma electron approaching a metallic boundary. The wavy line indicates the surface mode responsible for the attractive polarization potential (“image potential”) and  $L$  is the width of the “boundary layer” where a quantum-mechanical calculation applies. The electron loses (gains) energy due creation (annihilation) of electron-hole pairs in the metal. Due to these processes it may get trapped in (escape from) the bound states of the polarization potential. In other words, it may get stuck at (desorb from) the plasma boundary.  $W$  and  $E_F$  are, respectively, the work function and the Fermi energy of the metal.

electrons with a Fermi energy  $E_F$  and an infinitely high workfunction. The surface barrier is then also infinitely high, as in the model used in the previous section, and the single electron wavefunctions for an external and an internal electron,  $\Psi_{Qq}$  and  $\Phi_{Qq}$ , respectively, vanish at  $z = 0$  and are only defined in the respective halfspaces.

In analogy to the external single electron states, we write the internal single electron states as

$$\Phi_{\mathbf{K}k}(\mathbf{R}, z) = \frac{1}{\sqrt{A}} \exp[i\mathbf{K} \cdot \mathbf{R}] \phi_k(z) , \quad (36)$$

with  $\phi_k(z)$  the wavefunction for the vertical motion. It vanishes for  $z \geq 0$  and is a box-normalized standing wave for  $z < 0$ :

$$\phi_k(z) = \sqrt{\frac{2}{L}} \sin(kz) . \quad (37)$$

Using these states as a basis, the part of the Hamiltonian (35) describing the free motion of the elementary excitations of the boundary becomes

$$\mathcal{H}_s = \sum_{\mathbf{K}k} E_{\mathbf{K}k} D_{\mathbf{K}k}^\dagger D_{\mathbf{K}k} , \quad (38)$$

where  $D_{\mathbf{K}k}^\dagger$  creates an internal electron in the state  $\Phi_{\mathbf{K}k}$  with energy  $E_{\mathbf{K}k} = \hbar^2(K^2 + k^2)/2m_e$ . The interaction part of (35) can be written as

$$\mathcal{H}_{es} = \frac{1}{2} \sum_{QqQ'q' \mathbf{K}k \mathbf{K}'k'} \nu_{Q'q' \mathbf{K}'k'}^{Qq \mathbf{K}k} C_{Qq}^\dagger C_{Q'q'} D_{\mathbf{K}k}^\dagger D_{\mathbf{K}'k'} \quad (39)$$

**Table 2.** Fermi energy  $E_F$ , Fermi wavenumber  $k_F$ , and screening wavenumber  $(k_s)_{\text{bulk}}$  for various metals [69].

metal	$E_F[\text{eV}]$	$k_F[\text{\AA}]$	$(k_s)_{\text{bulk}}/k_F$
Ag	5.49	1.20	1.42
Cu	7.0	1.36	1.33
Al	11.7	1.75	1.17

with

$$\mathcal{V}_{\mathbf{Q}'q' \mathbf{K}'k'}^{\mathbf{Q}q \mathbf{K}k} = \frac{2\pi e^2}{A^2} \frac{\delta(\mathbf{Q} - \mathbf{Q}' + \mathbf{K} - \mathbf{K}')}{\sqrt{k_s^2 + (\mathbf{Q} - \mathbf{Q}')^2}} \times I_{qq'}^{(1)}(\mathbf{Q} - \mathbf{Q}') I_{kk'}^{(2)}(\mathbf{Q} - \mathbf{Q}') \quad (40)$$

and

$$I_{qq'}^{(1)}(\mathbf{R}) = \int_0^\infty dz \exp[-z\sqrt{k_s^2 + \mathbf{R}^2}] \psi_q^*(z) \psi_{q'}(z), \quad (41)$$

$$I_{kk'}^{(2)}(\mathbf{R}) = \int_0^\infty dz \exp[-z\sqrt{k_s^2 + \mathbf{R}^2}] \phi_k^*(-z) \phi_{k'}(-z) \quad (42)$$

where  $\mathbf{R} = \mathbf{Q} - \mathbf{Q}'$  is the lateral momentum transfer and  $k_s = (k_s)_{\text{surface}}$ , the screening wavenumber relevant for a Coulomb interaction between an external and an internal electron. Little is known about this parameter except that it should be less than the bulk screening wavenumber because the electron density in the vicinity of the boundary is certainly smaller than in the bulk. In [36] it was however argued, based on a comparison of experimentally and theoretically obtained branching ratios for positron trapping at and transmission through metal surfaces that most probably  $(k_s)_{\text{surface}} = 0.6(k_s)_{\text{bulk}}$ . Bulk screening wavenumbers for some metals are given in table 2.

Based on the Hamiltonian (35) with  $\mathcal{H}_s$  and  $\mathcal{H}_{es}$  given, respectively, by Eqs. (38) and (39), we will calculate in the next two sections for a metallic plasma boundary the electron sticking coefficient  $s_e$  and the electron desorption time  $\tau_e$ . Thereby it is implicitly assumed that the only effect the coupling to polarization-induced surface plasmons has is to give rise to an attractive potential  $V_p(z)$  supporting the external surface states in which physisorption takes place. The transitions between these states, that is, the physisorption kinetics itself, are triggered by the interaction with internal electrons.

In lowest order perturbation theory (see Fig. 6), the rate for transitions from a surface state  $(\mathbf{Q}'q')$  to a surface state  $(\mathbf{Q}q)$  is given by the golden rule:

$$\mathcal{W}(\mathbf{Q}q, \mathbf{Q}'q') = \frac{2\pi}{\hbar} \sum_{\mathbf{K}\mathbf{K}'} \sum_{kk'} |\mathcal{V}_{\mathbf{Q}'q' \mathbf{K}'k'}^{\mathbf{Q}q \mathbf{K}k}|^2 \times n_F(E_{\mathbf{K}'k'}) [1 - n_F(E_{\mathbf{K}k})] \times \delta(E_{\mathbf{Q}'q'} + E_{\mathbf{K}'k'} - E_{\mathbf{Q}q} - E_{\mathbf{K}k}), \quad (43)$$

where  $n_F(E) = 1/(\exp[(E - E_F)/kT_s] + 1)$  is the Fermi distribution function for the metal electrons with Fermi energy  $E_F$  and temperature  $T_s$ . Appropriately summed and weighted over initial and final states, the transition rate  $\mathcal{W}(\mathbf{Q}q, \mathbf{Q}'q')$  is the essential building block for the calculation of  $s_e$  and  $\tau_e$ .

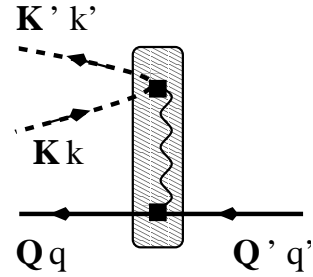


**Fig. 6.** Diagrammatic representation of the golden rule (43) for a transition from the surface state  $(\mathbf{Q}'q')$  to the surface state  $(\mathbf{Q}q)$  (solid lines) via scattering on an internal electron (dashed line) which can be interpreted as the coupling to internal electron-hole pairs. The wavy line denotes the screened Coulomb interaction between internal and external electrons and the box symbolizes the dynamic, that is, inelastic electron-metal interaction.

### 3.2 Sticking coefficient

In order to calculate the sticking coefficient  $s_e$  we consider the positive half space ( $z > 0$ ) as a kind of quantum-mechanical boundary layer. The probability  $S_{\mathbf{Q}n, \mathbf{Q}'q'}$  with which an electron approaching in an unbound state  $\Psi_{\mathbf{Q}'q'}$  the plasma-boundary at  $z = 0$  gets stuck in a bound state  $\Psi_{\mathbf{Q}n}$  is then given by the time it takes the electron to traverse the boundary layer forwards and backwards divided by the time it takes the electron to make a transition from  $\Psi_{\mathbf{Q}'q'}$  to  $\Psi_{\mathbf{Q}n}$  [37].

Since the width of the quantum-mechanical boundary layer is  $L$ ,

$$S_{\mathbf{Q}n, \mathbf{Q}'q'} = \frac{2L}{\text{in} \langle \mathbf{Q}'q' | \frac{\mathbf{p} \cdot \mathbf{n}}{m_e} | \mathbf{Q}'q' \rangle_{\text{in}}} \times \frac{1}{\mathcal{W}^{-1}(\mathbf{Q}n, \mathbf{Q}'q')}, \quad (44)$$

where the denominator in the first factor is the velocity matrix element calculated with the incoming part of the state  $\Psi_{\mathbf{Q}'q'}$ ;  $\mathbf{n}$  is the normal vector of the boundary pointing towards the plasma and  $\mathbf{p} = -i\hbar\nabla$ , the quantum-mechanical momentum operator. Using the asymptotic form of the unbounded wavefunctions given in Eq. (71) of appendix A, we find

$$\text{in} \langle \mathbf{Q}'q' | \frac{\mathbf{p} \cdot \mathbf{n}}{m_e} | \mathbf{Q}'q' \rangle_{\text{in}} = \frac{\hbar q'}{8m_e a_B}. \quad (45)$$

Hence,

$$S_{\mathbf{Q}n, \mathbf{Q}'q'} = \frac{16Lm_e a_B}{\hbar q'} \mathcal{W}(\mathbf{Q}n, \mathbf{Q}'q'). \quad (46)$$

The probability with which the electron approaching the boundary in the state  $\Psi_{\mathbf{Q}'q'}$  gets stuck in any one of the bound states – the energy resolved sticking coefficient – is then simply given by

$$S_{\mathbf{Q}'q'} = \sum_{\mathbf{Q}n} S_{\mathbf{Q}n, \mathbf{Q}'q'} = \frac{16Lm_e a_B}{\hbar q'} \sum_{n\mathbf{Q}} \mathcal{W}(\mathbf{Q}n, \mathbf{Q}'q'). \quad (47)$$

The sticking coefficient  $s_e$  entering the rate equation (2) is however an energy-averaged sticking coefficient resulting from an appropriately performed sum over  $S_{\mathbf{Q}'q'}$ . A rigorous derivation for  $s_e$  could be based on quantum-kinetic rate equations for the occupancies of the surface states [34, 35]. It takes, for instance, into account that the timescale for sticking is different from the timescale for desorption. A simpler way to obtain  $s_e$  is however to regard the wall as a particle detector. The global sticking coefficient can then be defined as

$$\sum_{\mathbf{Q}'q'} S_{\mathbf{Q}'q'} q' n_{\mathbf{Q}'q'} = s_e \sum_{\mathbf{Q}'q'} q' n_{\mathbf{Q}'q'} , \quad (48)$$

where  $n_{\mathbf{Q}'q'}$  are the occupancies of the unbound surface states  $\Psi_{\mathbf{Q}'q'}$ .

The occupancies  $n_{\mathbf{Q}'q'}$  depend on the properties of the plasma. It is tempting to simply identify  $n_{\mathbf{Q}'q'}$  with the incoming part of the electron distribution function as it arises on the surface from the solution of the Boltzmann-Poisson equations. However, one should keep in mind that the distribution function is a classical object whereas  $n_{\mathbf{Q}'q'}$  is a quantum-mechanical expectation value. There arises therefore the question how the quantum-mechanical processes encoded in the above equations can be properly fed into the semiclassical description of the plasma in terms of Boltzmann-Poisson equations. The issue is subtle because at the plasma boundary there is at least one potential, the surface potential, which varies so rapidly that the basic assumptions of the validity of the Boltzmann equation are no longer valid.

Mathematically, the microphysics should be put into a surface scattering kernel coarse-grained over a few nm which connects, generally retarded in time, the incoming electron distribution function with the outgoing one. But even for neutral particles, a microscopic derivation of such a scattering kernel has not yet been given. There exist only more or less plausible phenomenological expressions which parameterize the kernel, for instance, with sticking coefficients and desorption times [70].

From the boundary-layer point of view used in the derivation of Eqs. (44)–(48), the plasma, or, more precisely, the sheath of the plasma, is infinitely far away from the plasma boundary. Rigorously speaking, we can thus say nothing about how the microphysics at the plasma boundary merges with the physics in the plasma sheath.

To make nevertheless contact with the plasma we have to guess how the unbound surface states  $\Psi_{\mathbf{Q}q}$  are occupied. For simplicity we assume Maxwellian occupancy, with an electron temperature  $T_e = (k\beta_e)^{-1}$ , but other guesses, which might be more appropriate for the plasma sheath, are also conceivable. For Maxwellian electrons, the global sticking coefficient is given by

$$s_e = \frac{\sum_{\mathbf{Q}'q'} S_{\mathbf{Q}'q'} q' \exp[-\beta_e E_{\mathbf{Q}'q'}]}{\sum_{\mathbf{Q}'q'} q' \exp[-\beta_e E_{\mathbf{Q}'q'}]} . \quad (49)$$

In the limit  $L \rightarrow \infty$  and  $A \rightarrow \infty$  the momentum summations in Eqs. (44)–(49) become integrals. The calculation of  $S_{\mathbf{Q}'q'}$  and  $s_e$  reduces therefore to the calculation

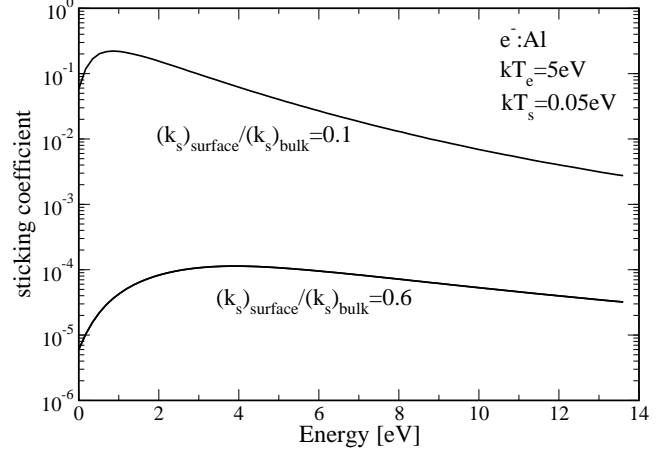


**Fig. 7.** Energy resolved sticking coefficient for a thermal beam of electrons with  $kT_e = 5\text{eV}$  hitting perpendicularly an aluminum surface at  $kT_s = 0.05\text{eV}$ . The screening wavenumber for the Coulomb interaction between an incident plasma electron and an internal aluminum electron,  $(k_s)_{\text{surface}}$ , is not well known. Results are therefore shown for  $(k_s)_{\text{surface}}/(k_s)_{\text{bulk}} = 0.1$  (weak screening, strong coupling) and for  $(k_s)_{\text{surface}}/(k_s)_{\text{bulk}} = 0.6$  (moderate screening, weak coupling);  $(k_s)_{\text{bulk}}$  is the screening wavenumber of aluminum (see table 2). Since  $(k_s)_{\text{surface}} = 0.6(k_s)_{\text{bulk}}$  is most probably the relevant screening parameter [36,39], the sticking coefficient is rather small.

of high-dimensional integrals. In appendix B we describe the approximations for the integrals we invoked in our exploratory calculation of the electron sticking coefficient. Although some of the integrals can then be done analytically, the final expressions for the sticking coefficients are still multi-dimensional integrals, which have to be treated numerically.

Measuring energies in units of  $R_0$  and length in units of  $a_B$ , Eq. (49) for the global sticking coefficient reduces to

$$s_e = \left(\frac{4}{\pi}\right)^2 \frac{\beta_e^{3/2}}{\beta_s^{1/2}} I_{\text{stick}} , \quad (50)$$

where

$$I_{\text{stick}} = \int_0^\infty dR \int_{-\infty}^\infty d\omega \frac{1 + n_B(\omega)}{1 + (R/k_s)^2} h(R, \omega) g(R, \omega) \quad (51)$$

with  $n_B(E) = 1/(\exp[\beta_s E] - 1)$  the Bose distribution function and  $h(R, \omega)$  and  $g(R, \omega)$  two functions containing, respectively, the electronic matrix elements (41) and (42). They are defined, respectively, in appendix B in Eq. (90) and (91).

Below we also present results for the energy resolved sticking coefficient for perpendicular incidence ( $\mathbf{Q}' = 0$ ). It is given by

$$S_{E'}^\perp = \left(\frac{4}{\pi}\right)^2 \frac{\pi^{1/2}}{\beta_s^{1/2}} \int_0^\infty dR g^\perp(R, E') , \quad (52)$$

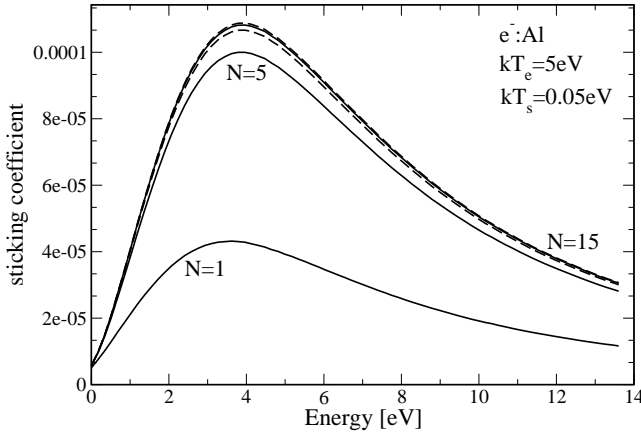


**Fig. 8.** Dependence of the energy resolved sticking coefficient for perpendicular incidence on the number  $N$  of bound states included in the calculation. Except of the screening wavenumber, which is set to  $(k_s)_{\text{surface}} = 0.6(k_s)_{\text{bulk}}$ , the parameters are identical to the ones used in Fig. 7. The dashed lines are for  $N = 10$  and  $N = 20$ , respectively, indicating the fast converge with respect to  $N$ .

with  $E' = q'^2$  and  $g^\perp(R, E')$  a function defined in Eq. (93) in appendix B.

The functions  $h(R, \omega)$ ,  $g(R, \omega)$ , and  $g^\perp(R, E')$  contain summations over the Rydberg series of bound surface states. If not stated otherwise, we truncated these sums after  $N = 15$  terms. These functions are moreover only defined in terms of integrals which have to be done numerically. We use Gaussian integration with 40–80 integration points. More specifically,  $h(R, \omega)$  and  $g^\perp(R, E')$  are one-dimensional integrals and  $g(R, \omega)$  is a two-dimensional one. Hence,  $s_e$  and  $S_E^\perp$  are, respectively, given by a five-dimensional and a two-dimensional integral.

In the formulae for the sticking coefficients we multiplied the binding energies of the surface states  $|E_n|$  obtained from Eq. (30) by an overall factor of 0.7. This value was chosen to bring the binding energy of the lowest surface state  $|E_1| = 0.85\text{eV}$  in accordance with the experimentally measured value for copper:  $|E_1|^{Cu} \approx 0.6\text{eV}$  [48]. For other metals we used the same correction factor.

Figure 7 shows the results for  $S_E^\perp$ , when a thermal beam of electrons with  $kT_e = 5\text{eV}$  perpendicularly hits an aluminum boundary at  $kT_s = 0.05\text{eV}$ . We plotted data for  $(k_s)_{\text{surface}}/(k_s)_{\text{bulk}} = 0.1$  (weak screening, strong coupling) and for  $(k_s)_{\text{surface}}/(k_s)_{\text{bulk}} = 0.6$  (moderate screening, weak coupling). The latter is the screening parameter used in [36,39] to study the interaction of positrons with an aluminum surface. If the corresponding value for  $1/(k_s)_{\text{surface}}$  is indeed a reasonable estimate for the length on which the Coulomb interaction between an external and an internal electron is screened, the sticking coefficient for electrons should be extremely small, of the order of  $10^{-4}$ . Only for weak screening, and thus strong coupling, does  $S_E^\perp$  approach values of the order of  $10^{-1}$  which are perhaps closer to the value one would on first sight expect.

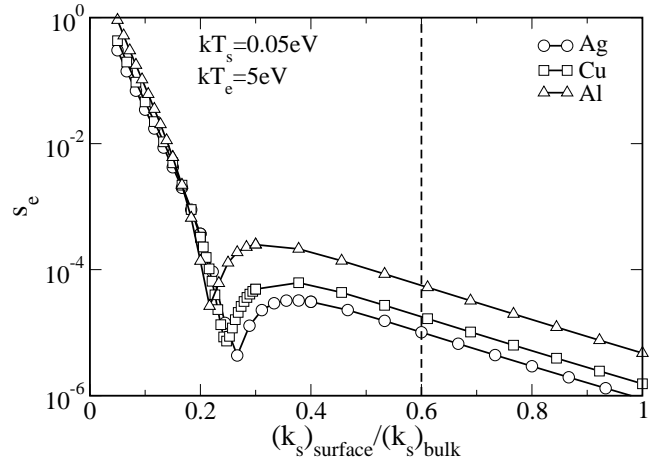


**Fig. 9.** The global sticking coefficient  $s_e$  for a thermal beam of electrons with  $kT_e = 5\text{eV}$  hitting various metal surfaces at  $kT_s = 0.05\text{eV}$  as a function of  $(k_s)_{\text{surface}}/(k_s)_{\text{bulk}}$ , where  $(k_s)_{\text{bulk}}$  is the screening wavenumber in the bulk of the respective metal (see table 2). Following [36,39], we would expect  $(k_s)_{\text{surface}} = 0.6(k_s)_{\text{bulk}}$  to be a reasonable estimate for the screening parameter. Hence,  $s_e \approx 10^{-5} - 10^{-4}$ .

In order to clarify the contribution the various bound states have to the sticking coefficient, we plot in Fig. 8 the dependence of  $S_E^\perp$  on the number  $N$  of bound states included in the calculation. As can be seen, the lowest bound state ( $N = 1$ ) contributes only roughly 40% to the total  $S_E^\perp$ . The sticking coefficient increases then with increasing  $N$  but converges for  $N \approx 10 - 20$ . Because of this fast convergence we present all results below only for  $N = 15$ . The reason for the convergence can be traced back to the decrease of the electronic matrix element  $I_{kn}^{(1)}(\mathbf{R})$  defined in Eq. (41), which we approximate by  $I_{k \ll 1n}^{(1)}(\mathbf{R} = 0)$  (see appendix B), with increasing  $n$ , where  $n = 1, 2, \dots$  labels the bound surface states.

Global sticking coefficients  $s_e$  as a function of the screening wavenumber  $(k_s)_{\text{surface}}$  are shown in Fig. 9 for different metals. For  $(k_s)_{\text{surface}}/(k_s)_{\text{bulk}} > 0.4$ , the sticking coefficients are again extremely small. As expected they increase with decreasing  $(k_s)_{\text{surface}}/(k_s)_{\text{bulk}}$ , reaching values close to unity for weak screening. In this strong coupling regime, our perturbative calculation of  $s_e$  is no longer valid. We believe however that  $(k_s)_{\text{surface}}/(k_s)_{\text{bulk}} < 0.4$  is unphysical. The kink around  $(k_s)_{\text{surface}}/(k_s)_{\text{bulk}} \approx 0.25$  must be due to an accidental resonance in  $g(R, \omega)$ . It is of no physical significance.

Why is the sticking coefficient for electrons so small? We have no satisfying explanation except that our calculation produces just that. The approximations we had to make to end up with manageable equations for  $s_e$ , in particular, the assumptions about the momentum dependence of the electronic matrix elements (see appendix B and, for a discussion, the next section) should at most lead to a sticking coefficient which is perhaps one order of magnitude off, but not three. In this respect we emphasize that in contrast to the calculations performed in [36,

39] for a positron, which produce positron sticking coefficients of the order of 0.1, we use the eigenenergies and eigenstates of the  $1/z$  potential and not the ones of an artificial box potential. Usually it is assumed that  $s_e$  is also at least of the order of 0.1 [61]. This expectation seems to be however primarily based on the semiclassical back-on-the envelop-estimate of Umebayashi and Nakano [71]. It is thus appropriate to discuss their approach in some detail.

From the energy  $\Delta E_s$  an electron can exchange in a single classical collision with the constituents of the solid they first estimated, using the analogy to the Mössbauer effect, the probability  $\alpha$  for inelastic one-phonon emission. For that purpose, they had to estimate the number  $N_c$  of constituents of the surface an electron with a de-Broglie wavelength corresponding to its kinetic energy  $E_0$ ,  $\lambda_e^{dB} = 2\pi a_B \sqrt{R_0/E_0}$ , simultaneously impacts. A rough estimate is  $N_c = (\lambda_e^{dB}/a)^2$ , where  $a$  is the lattice constant of the material. Under the assumption that the electron hops along the surface they then calculated the probability with which the electron does not escape after  $l$  hops where  $l$  is the number of inelastic collisions which are necessary for the electron to transfer its whole positive kinetic energy to the lattice, that is, to end up in a state of negative energy. Identifying this probability with the (global) sticking coefficient, they obtained

$$s_e = \prod_{i=0}^{l-1} \frac{1}{1 + \beta_i/\alpha} , \quad (53)$$

where  $\beta_i = (E_0 - i\Delta E)/E_b$  is the escape probability after  $i$  inelastic collisions [72],  $\Delta E = 2\Delta E_s/3N_c\alpha$ ,  $\Delta E_s = 4m_e(E_0 + E_b)/M$ ,  $E_b$  is the depth of the surface potential and  $M$  is the mass of the constituents of the solid.

Sticking coefficients for graphite obtained from Eq. (53) are shown in Fig. 10. Within Umebayashi and Nakano's semiclassical approach we identified  $E_b$  with the binding energy of the electron. As can be seen from Fig. 10 the sticking coefficient very quickly approaches extremely small values with increasing energy  $E_0$ . The smaller the binding energy  $E_b$ , the faster the decrease. The values for  $s_e$  originally given by Umebayashi and Nakano were only for kinetic energies smaller than 0.0026 eV and binding energies larger than 1 eV. Only in this parameter regime is the sticking coefficient close to one. In the parameter range which is of most interest to us (kinetic and binding energies of at least a few tenth of an electron volt) Umebayashi and Nakano's estimate gives also an extremely small sticking coefficient.

We should of course not directly compare the results obtained from Eq. (50) with the ones obtained from Eq. (53) because Eq. (50) assumes energy relaxation due to internal electron-hole pairs whereas Eq. (53) assumes energy relaxation due to phonons. However, a quantum-mechanical calculation of the phonon-induced electron sticking coefficient at zero lattice temperature also shows that  $s_e \approx 10^{-4}$  [38], in contrast to what Umebayashi and Nakano find. Although they incorporate some quantum mechanics their approach is basically classical. It is based on the notion of a classical particle hopping around on the surface

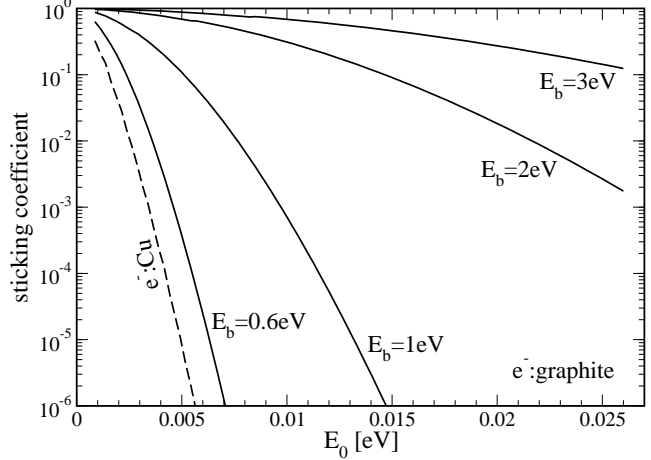


**Fig. 10.** Electron sticking coefficient obtained from Umebayashi and Nakano's phenomenological model [71], see Eq. (53). The solid lines are for the  $e^-$ :graphite system originally considered by them ( $kT_D = 420K$ ,  $M_C = 12m_p$ , where  $m_p$  is the proton mass, and  $a = 2.5\text{\AA}$ ) and the dashed line is for an  $e^-$ :Cu system ( $E_b = 0.6\text{eV}$ ,  $kT_D = 343K$ ,  $M_{Cu} = 64m_p$ , and  $a = 3.61\text{\AA}$ ). The sticking coefficient diminishes rapidly with increasing electron energy and approaches one at zero electron energy, in contrast to what one would expect from a quantum-mechanical calculation [38].

and exchanging energy with the solid in binary encounters. As in any classical theory for the sticking coefficient, it is therefore not surprising that the sticking coefficient they obtain approaches unity for the low energies they consider [35].

### 3.3 Desorption time

We now calculate the electron desorption time  $\tau_e$ . For that purpose, we have to specify the occupancies of the bound electron surface states. In general, this is a critical issue. However, provided the desorption time  $\tau_e$  is much larger than the time it takes to establish thermal equilibrium with the boundary, it is plausible to assume that bound electron surface states are populated according to

$$n(\mathbf{Q}n) \sim \exp[-\beta_s E_{\mathbf{Q}n}] , \quad (54)$$

where  $T_s = 1/k\beta_s$  is the surface temperature.

Desorption is accomplished as soon as the electron is in any one of the unbound surface surface states. Hence, the inverse of the desorption time, that is, the desorption rate, is given by [35]

$$\frac{1}{\tau_e} = \frac{\sum_{\mathbf{Q}'n'} \sum_{\mathbf{Q}q} \exp[-\beta_s E_{\mathbf{Q}'n'}] \mathcal{W}(\mathbf{Q}q, \mathbf{Q}'n')}{\sum_{\mathbf{Q}n} \exp[-\beta_s E_{\mathbf{Q}n}]}, \quad (55)$$

where  $\mathcal{W}(\mathbf{Q}q, \mathbf{Q}'n')$  is the transition rate from the bound surface state  $(\mathbf{Q}', n')$  to the unbound surface state  $(\mathbf{Q}, q)$  as defined by the golden rule (43).

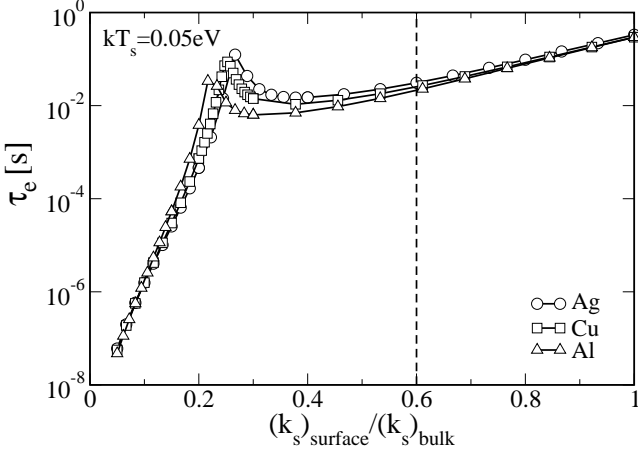


**Fig. 11.** Desorption time  $\tau_e$  for an electron bound in the polarization-induced external surface states of various metal surfaces at  $kT_s = 0.05\text{eV}$  as a function of  $(k_s)_{\text{surface}}/(k_s)_{\text{bulk}}$ . Since  $(k_s)_{\text{surface}} = 0.6(k_s)_{\text{bulk}}$  is most probably the relevant screening wavenumber [36, 39],  $\tau_e \approx 10^{-2}\text{s}$ . For the used material parameters, see table 2.

Measuring again energies in units of  $R_0$  and lengths in units of  $a_B$  and using the same approximations as in the calculation of the sticking coefficient (see appendix B) the desorption rate can be cast into

$$\tau_e^{-1} = \frac{R_0}{2\pi^3\hbar Z} I_{\text{desorb}}, \quad (56)$$

where

$$I_{\text{desorb}} = \int_0^\infty dR \int_{-\infty}^\infty d\omega \frac{1 + n_B(\omega)}{1 + (R/k_s)^2} f(R, \omega) g(R, \omega), \quad (57)$$

$Z = \sum_n \exp[-\beta_s E_n]$ ,  $n_B(E)$  is again the Bose distribution function, and  $f(R, \omega)$  is a function defined in appendix B in Eq. (97) in terms of an one-dimensional integral. Thus, to obtain  $\tau_e^{-1}$  from Eq. (56) we have to do a five-dimensional integral. As for the calculation of  $s_e$  we again use Gaussian quadratures for that purpose.

In Figure 11 we present, as a function of the screening parameter, numerical results for  $\tau_e$  for an electron bound in the polarization-induced external surface states of various metal surfaces at  $kT_s = 0.05\text{eV}$ . To be close to reality, we again corrected the binding energies  $|E_n|$  by a factor 0.7. As can be seen, except for small screening parameters and thus strong coupling,  $\tau_e \approx 10^{-2}\text{s}$ .

Compared to typical desorption times for neutral molecules, which are of the order of  $10^{-6}\text{s}$  or less [35], the electron desorption time we find is rather long. This is a consequence of our assumption that the bound electron is in thermal equilibrium with the surface (viz: Eq. (54)) and the fact that the binding energy of the lowest surface state  $|E_1| \gg kT_s$ . Thus, the electron desorbs de facto from the lowest surface state which has a binding energy of  $\sim 0.6\text{eV}$ . The binding energies for neutral molecules, on the other hand, are typically one order smaller and thus of

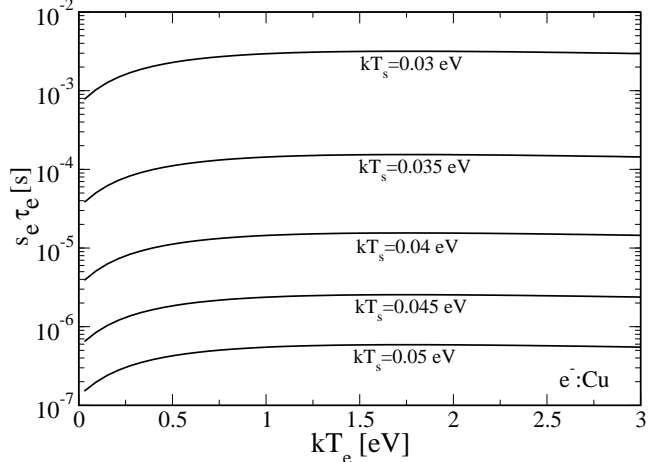


**Fig. 12.** The product  $s_e \tau_e$  as a function of  $kT_e$  for a thermal beam of electrons hitting a copper surface at various temperatures  $kT_s$ . The surface screening wavenumber is set to  $(k_s)_{\text{surface}} = 0.6(k_s)_{\text{bulk}}$ , where  $(k_s)_{\text{bulk}}$  is the screening wavenumber for copper (see table 2).

the order of  $kT_s$  resulting in much larger desorption rates and thus shorter desorption times.

In the model for the quasi-stationary charge of a dust particle presented in the previous section the product  $(s\tau)_e$  was of central importance. The microscopic theory for metallic grains just developed gives

$$(s\tau)_e = \frac{h}{(kT_e)^{3/2}(kT_s)^{-1/2}} \frac{16I_{\text{stick}}}{I_{\text{desorb}}} \sum_n \exp[\beta_s |E_n|], \quad (58)$$

where  $I_{\text{stick}}$  and  $I_{\text{desorb}}$  are defined in Eqs. (51) and (57), respectively.

Figure 12 shows numerical results for  $(s\tau)_e$  for a copper surface as a function of the electron and surface temperature. The screening wavenumber  $(k_s)_{\text{surface}} = 0.6(k_s)_{\text{bulk}}$  and the binding energies are again corrected by the factor 0.7 which makes  $|E_1|$  to coincide with the experimental value for copper. Notice, the weak dependence of the product  $(s\tau)_e$  on the electron temperature and the rather strong dependence on the surface temperature. The latter is of course a consequence of the exponential function in Eq. (58). Although the sticking coefficient and desorption times have values which are perhaps in contradiction to naive expectations,  $s_e$  being extremely small and  $\tau_e$  being rather large, the product  $(s\tau)_e$  has the order of magnitude we would expect from our surface model (see section 2). In particular,  $(s\tau)_e$  for  $kT_s = 0.045\text{eV}$  would produce grain charges of the correct order of magnitude. Thus, using Eq. (58) instead of Eq. (13) and  $kT_s$  as an adjustable parameter, which is still necessary because the grain temperature is unknown, we could produce, for physically realistic surface temperatures, surface charges for metallic grains which are in accordance with experiment [19].

Although the microscopic Eq. (58) has a similar structure as the phenomenological expression (13) there are significant differences. First, the microscopic formula con-

tains more than one bound state and depends not only on  $T_s$  but also on  $T_e$ . In addition, there is a numerical factor  $16 = 2 \times 8$  where the factor 2 comes from the fact that an electron traversing the quantum-mechanical boundary layer can make a transition to a bound state on its way towards the surface and on its way back to the plasma and the factor 8 originates from the asymptotic form of the wavefunction for the incoming electron. The phenomenological approach simply assumes here a plane wave whereas the microscopic approach works with Whittaker functions (see appendix A and B). Most importantly, however, the two functions  $I_{\text{stick}}$  and  $I_{\text{desorb}}$ , which depend on the microscopic details of the inelastic scattering process driving physisorption, and thus on the electron and surface temperature as well as material parameters such as, for instance, the screening wavenumber, are in general not identical.

For the hypothetical case of a single bound state, however, whose binding energy  $|E_1|$  is much smaller than  $kT_s$  and  $kT_e$ , Eq. (58) reduces to a form which becomes, except of the numerical factor referred to in the previous paragraph, identical to the phenomenological expression (13) for  $kT_e = kT_s$ . The simplification arises because for low temperatures the integrals defining  $I_{\text{stick}}$  and  $I_{\text{desorb}}$  can be calculated asymptotically within Laplace's approximation (see appendix B). The sticking coefficient and desorption time are then given by

$$s_e^L = \frac{4|I_1^{(1)}|^2 \bar{g}}{\pi \beta_s^{1/2} \beta_e^{1/2}}, \quad (59)$$

$$\tau_e^L = 8\pi^2 \beta_s^2 \frac{\hbar}{R_0} \frac{\exp[\beta_s |E_1|]}{|I_1^{(1)}|^2 \bar{g}}, \quad (60)$$

with  $\bar{g}$  defined in Eq. (104) in appendix B. Thus, the product,

$$(s\tau)_e^L = \frac{16\hbar}{(kT_s)^{3/2} (kT_e)^{-1/2}} \exp[\beta_s |E_1|], \quad (61)$$

is independent of the microscopic details of the inelastic scattering processes encoded in  $|I_1^{(1)}|^2 \bar{g}$ . Identifying  $|E_1|$  with the electron desorption energy  $E_e^d$  and setting  $kT_e = kT_s$ , we finally obtain, except of the numerical factor  $16 = 8 \times 2$ , from Eq. (61) the phenomenological expression (13).

Using Eqs. (59)–(61) we find for an electron at a copper boundary with  $kT_e = kT_s = 0.045\text{eV}$ ,  $s_e^L = 6.23 \times 10^{-6}$ ,  $\tau_e^L = 0.131\text{s}$ , and  $(s\tau)_e^L = 8.17 \times 10^{-7}\text{s}$ . Taking only one bound state into account, the corresponding values obtained from Eqs. (50) and (56) are  $s_e = 4.42 \times 10^{-6}$  and  $\tau_e = 0.135\text{s}$ , which leads to  $(s\tau)_e = 6 \times 10^{-7}\text{s}$ , indicating that at low temperatures Laplace's approximation works indeed reasonably well. Since  $\tau_e$  does not depend on  $kT_e$  and  $kT_s$  is usually much smaller than  $|E_1|$ , approximation (60) for  $\tau_e$  can be actually always applied, provided the assumption is correct, that the electron is initially in thermal equilibrium with the surface and hence basically in its lowest bound state. The approximation (59) for  $s_e$ , on the other hand, deteriorates quickly with increasing electron temperature, as does the approximation (61) for  $(s\tau)_e$ .

That the microscopic expression (58) can be reduced to the phenomenological expression (13) is a consequence of the perturbative calculation of  $s_e$  and  $\tau_e$  using the golden rule transition rate  $\mathcal{W}(\mathbf{Q}q, \mathbf{Q}'q')$  which obeys detailed balance. In this respect, our calculation is on par with Lennard-Jones and Devonshire's original microscopic derivation of the product  $(s\tau)_e$  [30]. However, in contrast to them, our model is three-dimensional and not one-dimensional and the elementary excitations of the solid we consider are electron-hole pairs and not phonons. It is thus reassuring that we are able to extract, under the conditions specified above and except of a numerical factor, whose origin is however clear, from our microscopic calculation of  $s_e$  and  $\tau_e$  the relation (13) we used in [29] to have a first estimate for  $(s\tau)_e$ .

## 4 Critique

In the previous section we demonstrated for a particular case, a metallic boundary with electron energy relaxation due to creation and annihilation of internal electron-hole pairs, how a quantum-mechanical calculation can be set up to obtain  $s_e$  and  $\tau_e$  from a microscopic model for the electron-wall interaction. To obtain manageable equations we had to make various approximations, some were purely technical, but others concerned the physics. We now restate and criticize the approximations in the hope to turn it to a list of to-do's.

We start with the purely technical approximations concerning the calculation of the electronic matrix elements which arise when we take internal electron-hole pairs of the metal to be responsible for electron energy relaxation at metallic plasma boundaries. For other mechanisms and other materials, other matrix elements appear which require other approximations.

In the calculation of the transition rate  $\mathcal{W}(\mathbf{Q}'q', \mathbf{Q}, q)$  we neglected the dependence of the matrix elements (41) and (42) on the lateral momentum transfer  $\mathbf{R}$  and approximated furthermore  $I_{kn}^{(1)}(\mathbf{R} = 0)$  by its leading term for  $k \ll 1$ . Both approximations can be avoided but the final equations become more complex and the costs for their numerical handling accordingly higher. At the present stage of the investigation this seemed to us not justified. Even more so because we do not believe that these approximations are the cause for the unexpectedly small values for  $s_e$  and the unexpectedly large values for  $\tau_e$ . Neglecting the dependence on the lateral momentum overestimates even the matrix elements, hence the transition rate, and thus, eventually,  $s_e$  and  $\tau_e^{-1}$ . The ignored nonlinear  $k$ -dependence of  $I_{nk}^{(1)}(0)$  (see Eq. (79) in appendix B), on the other hand, cannot be so large that it increases  $\mathcal{W}(\mathbf{Q}'q', \mathbf{Q}, q)$  by three orders of magnitude as it would be required to obtain  $s_e \sim 0.1 - 1$  and  $\tau_e \sim 10^{-5} - 10^{-6}\text{s}$ , the values one would perhaps naively expect.

Nevertheless, a full calculation is desirable because a small  $s_e$  would have even implications for the canonical description of the formation of quasi-stationary surface charges at plasma boundaries. For instance, the precursor

to Eq. (4),  $s_e j_e^{\text{plasma}}(Z_p) = s_i j_i^{\text{plasma}}(Z_p)$ , would definitely not give reasonable surface charges  $Z_p$  except  $s_i$  is also rather small. But this in turn would imply that ions are trapped in the shallow states of the Coulomb potential, and hence in a space charge region in front of the surface, in accordance with what we expect, but contrary to the view of others [52, 53, 54].

Both the electron sticking coefficient  $s_e$  and the electron desorption  $\tau_e$  were obtained from the golden rule for transitions between surface states. This is of course only justified for weak coupling. There is however no principal problem to go beyond the golden rule using techniques from many-body theory.

For the calculation of the desorption time we assumed that the electron is in thermal equilibrium with the surface, that is, that the desorption time is much larger than the timescale on which thermal equilibrium at the surface is established. In that case, the electron basically desorbs from the lowest bound state. Although the  $\tau_e$  we obtain is consistent with the equilibrium assumption it does not justify it. For that purpose, the calculation of the desorption time has to be based on quantum-kinetic rate equations for the time evolution of the occupancies of the surface states [34, 35].

The approach layed out in the previous section has to be significantly modified, when the elementary excitations of the solid have not enough energy to couple the lowest bound surface states to the continuum. In that case, the cascade model developed by Gortel and coworkers [32] has to be used. Its main idea is that an electron initially bound in deep states can successively climb up to the continuum using weaker bound states as intermediaries. Technically, the approach is also based on rate equations for the occupancies of the surface states.

For metals electron-hole pairs should provide the most efficient relaxation channel, with phonons and other elementary excitations being unimportant, because their energy is either too high (plasmons) or too low (phonons). Both leads to severe restrictions in the available phase space. For dielectric boundaries, however, it is the energy of internal electron-hole pairs which is too high for having any effect. Electron energy relaxation should then be primarily driven by phonons. Their energy, however, is in the cases of interest, for instance, graphite or silicon, too low for promoting an electron from the lowest surface states all the way up to the continuum. Hence,  $s_e$  and  $\tau_e$  have to be calculated from Gortel *et al.*'s cascade model. When the energy of the phonon is even not enough to connect two neighboring bound states, the transition rates entering the rate equations have to be moreover obtained from a generalized expression [31, 35] which takes multiphonon processes into account. Multiphonon processes should play a role even for graphite boundaries, where the Debye energy is rather high, but not high enough to couple the two lowest bound states to each other (see table 1). This coupling, however, is expected to be the rate-limiting one, that is, the one which eventually determines the electron desorption time.

In our model we made the overall assumption that plasma electrons cannot enter the plasma boundary. In principle, however, electrons with an energy larger than the projected energy gap of the solid [73], can enter the plasma boundary, scatter inside the material, before bouncing back to the surface, where they may be either re-emitted to the plasma or trapped in internal or external bound states. Since we used an infinitely high surface barrier, assuming the projected energy gap is much larger than the typical energy of the plasma electrons, processes inside the material were not included in our model.

Here, we come to a potentially very interesting point as far as metallic boundaries are concerned. The projected energy gap for metal surfaces depends strongly on the crystallographic orientation of the surface. Plasma boundaries are however not the well prepared surfaces typically used in the investigations of surface states [42, 43, 44, 45, 46, 47, 48, 49, 50, 51]. In addition, they usually have a curvature. Thus, plasma boundaries will almost certainly never coincide with a crystallographic plane. Hence, the projected energy gap will vary along the boundary. Regions can be thus expected where external surface states are more robust than in others. It is open how all this affects, for instance, the homogeneity of surface charges at metallic plasma boundaries.

For dielectric boundaries the projected energy gap is of the order of the energy gap of the bulk material and should not depend strongly on the crystallographic plane of the surface. But a problem which concerns both metallic and dielectric surfaces is surface roughness. In our model the plasma boundary is a well-defined mathematical plane. On the atomistic scale, and we actually do calculations on this scale, the surface is however not perfect. In a refined model for surface states this has to be taken into account.

We also assumed that the residual dynamical interaction between an approaching electron and the polarization mode it induces does not annihilate the existence of external surface states. Although the exact surface potential, from which surface states should be calculated, is not known, experimentally, surface states have been detected many times [40, 41, 42, 43, 44, 45, 46, 47, 48, 49, 50, 51]. In the exploratory calculation presented in this paper, we used therefore the simplest potential which contains the essential physics and yet allows an analytical calculation of wavefunctions and matrix elements. With variational techniques the static potential could be however improved. In particular, it would be possible to deduce a potential, which has a finite value at the boundary. Within this approach, the lifetime of surface states due to residual interactions could be also calculated.

An alternative to the model Hamiltonian (22) is to calculate from ab-initio the surface potential for a given plasma boundary. This is however illusionary even when the boundary would be crystallographically well defined. The quantum-mechanical exchange and correlation effects are extremely hard to incorporate in a local-density approximation, the work-horse of most ab-initio packages for electronic structure calculations for solids. Precisely these effects however make the image plane not to coin-

cide with the surface, that is, which force the potential to saturate at the boundary. In principle, this effect could be mimicked by making the potential constant for distances smaller than a critical distance and use the critical distance as an adjustable parameter to fit experimental data. But even for the classical image potential this strategy would lead to a Schrödinger equation which could not be solved analytically anymore.

Quite generally, to short-circuit unknown microscopic details of plasma boundaries, one could work with a model potential amenable to an analytical treatment of the problem and containing adjustable parameters which are used to reproduce experimentally measured quantities, for instance, the binding energies of surface states. However, experimental techniques suitable for probing surface states, for instance, inverse photoemission spectroscopy, have not yet been used to explore the electronic microphysics at the plasma boundary. Even measurements of the surface charge (or potentials) are rare. Surface charges have been measured in dielectric barrier discharges [20, 21, 22, 23] and of course, in complex plasmas, where various techniques can be invoked to determine the charge of floating  $\mu\text{m}$ -sized dust particles [13, 14, 15, 16, 17, 18, 19]. But even there are the data not complete. Most importantly, although the particle temperature has been recently measured [67] the particle temperature and the particle charge have not yet been measured simultaneously. For the microscopic modeling of surface charges we propose it is however important to know both quantities.

We did not say much about ions, hinting only that, in principle, the ion kinetics in front of a floating inert plasma boundary can be interpreted as a physisorption process in the attractive floating potential of the negatively charged boundary. How strong the ion is bound to the surface (ion desorption energy), and thus how close it can come to it, as well as its sticking coefficient and desorption time, depend on the efficiency of plasma-based inelastic scattering processes to force the ion down or up the Rydberg series of the floating potential. Of course, the ion cannot come closer than its radius. The polarization-induced part of the ion potential plays thus not such an important role as for electrons, at least, when the boundaries already collected some charge. Within this scenario, we imagine ions to be trapped in a space charge zone, a few micrometers away from the boundary. At the moment, this is however only a hypothesis. A detailed study of the ion kinetics – using either quantum-mechanical techniques borrowed from the theory of physisorption, as we suggest, or using classical simulations – can show if the hypothesis (which does only affect the constituting equation for the surface charge and not the calculation of  $s_e$  and  $\tau_e$ ) is correct or not.

## 5 Concluding remarks

In this colloquium we proposed to treat the interaction of charged plasma particles with inert plasma boundaries, that is, boundaries which stay intact during their exposure to the plasma, as a physisorption process involving external surface states. The sticking coefficients  $s_{e,i}$  and

desorption times  $\tau_{e,i}$  can then be calculated from a microscopic model which contains (i) the static potential supporting bound and unbound surface states and (ii) the coupling of these states to an environment which triggers transitions between them. Microscopically, the sticking of a plasma particle to the surface corresponds then to a transition from an unbound surface state to a bound one. Desorption of a particle from the wall is then simply the reverse process.

Although this point of view can be applied to ions and electrons, we worked it out only for electrons because the surface states for electrons are surface states in the ordinary sense, that is, states which are only a few  $\text{nm}$  away from the surface. Hence, the environment responsible for transitions between electronic surface states, and thus for sticking and desorption of an electron, are the elementary excitations of the solid. For ions, however, as soon as the surface collected some electrons, the surface potential is the long-range attractive Coulomb potential. Sticking and desorption of ions occurs thus far away from the surface. Nevertheless, provided the surrounding plasma is taken as the environment triggering transitions between ion surface states, the dynamics and kinetics of ions in front of the boundary can be described in close analogy to the electron dynamics and kinetics occurring much closer to the surface. Since without the surface no attractive Coulomb potential for ions would exist, the ion dynamics and kinetics is also a kind of surface physics although it takes place far away from the surface.

The physisorption kinetics also determines the average distance of a particle from the surface. This distance is a quantum-mechanical expectation value and can thus be calculated from the quasi-stationary solution of the rate equations for the occupancies of the bound surface states. We did not yet do such a calculation. But it is planned because it would verify or falsify our expectation that ions in an almost collisionless plasma pile up in front of a spherical grain. The affirmative case would strongly support our surface model for the grain charge. It would however also have significant consequences for electron-ion recombination, the most important heat source for the particle, because, spatial separation, even if it is only on the microscopic scale, would affect the recombination probability  $\alpha_R$ .

Admittingly, the microphysics at the plasma-boundary we discuss is not the one utilized in plasma technology. Precisely the processes we excluded are most important there: Implantation of heavy particles, reconstruction or destruction of the surface due to high energy particles, and chemical modification due to radicals, to name just a few. The target surfaces are of course charged but, from the perspective of plasma technology, the surface charges only control the particle fluxes to the surfaces. Properties other than their mere existence are of no concern.

From a microscopic point of view, the technologically important surface processes just listed are extremely complicated. A description of these processes at a level, let say, we are used to describe superconductivity in bulk metals is certainly far from reach. It may even not be required

for plasma technology to proceed as a business. But as in other branches of science, it is the pleasure and duty of curiosity driven plasma research to push the understanding of particular processes, technologically relevant or not, to an ever increasing level of sophistication. We firmly believe, the microphysics at an inert plasma boundary is now ready for a truly microscopic understanding. It is our hope to have inspired other groups joining us on our journey to the microphysics at an inert plasma boundary. In particular, however, we hope to have found experimentalists eager to design experiments with well-defined model surfaces, which come as close as possible to the idealized boundaries theorists have to consider in their calculations, and at the same time are accessible to the surface diagnostics used elsewhere in surface science.

## A Electronic wavefunctions and matrix elements

In this appendix we summarize the properties of the electronic wavefunctions for the vertical motion of the external electron. The results are well-known and the appendix primarily serves the purpose to fix our notation.

First, we consider bound surface states. Using  $y = z/2a_B n$ , with  $n = 1, 2, \dots$  the quantum number labelling the Rydberg series of bound states, the Schrödinger equation (30) for the vertical motion becomes

$$\frac{d^2}{dy^2} \psi_n(y) + \left[ -\frac{1}{4} + \frac{n}{y} \right] \psi_n(y) = 0 , \quad (62)$$

whose solutions are Whittaker functions [74]. Hence, the wavefunctions which vanish at  $z = 0$  and for  $z \rightarrow \infty$  are

$$\psi_n(z) = N_n W_{n,1/2}(y) = \exp[-y/2] y^{(-n-1)} (n-1)! L_{n-1}^{(1)}(y) , \quad (63)$$

where  $N_n$  is a normalization constant and  $L_{n-1}^{(1)}(y)$  is an associated Laguerre polynomial. The corresponding eigenvalues are  $E_n = -R_0/16n^2$ .

In order to find the normalization constant, we insert the expansion of the Whittaker function [74],

$$W_{n,1/2}(y) = \exp[-y/2] y^n \sum_{q=0}^n a_q y^{-q} , \quad (64)$$

where

$$a_q = \frac{(-)^q}{q!} \frac{\Gamma(n+1)\Gamma(n)}{\Gamma(n-q)\Gamma(n-q+1)} \quad (65)$$

with  $\Gamma(n)$  the Gamma function, in the normalization integral,

$$1 = \int_0^\infty dz |\psi_n(z)|^2 . \quad (66)$$

Term-by-term integration leads then to

$$N_n = \sqrt{\frac{1}{4n^3 \Gamma(n)^2 a_B}} = \frac{\mathcal{N}_n}{\sqrt{a_B}} , \quad (67)$$

which is the defining equation for  $\mathcal{N}_n$  needed in appendix B.

For the continuum states, we use  $y = ikz/2a_B$  as an independent variable. The Schrödinger equation (30) can then be reduced to (62) with  $n$  replaced by  $-ik^{-1}$ . The continuum states with energy  $E_k = R_0 k^2/16$  which vanish at  $z = 0$  are thus given by [74]

$$\psi_k(z) = N_k M_{-ik^{-1},1/2}(y) . \quad (68)$$

As for any continuum state, to find the normalization constant  $N_k$  is somewhat tricky. We could normalize  $\psi_k(z)$  on the momentum scale but we found it more convenient to use a box-normalization considering the plasma halfspace ( $z > 0$ ) as a slab of width  $L$  with  $L \rightarrow \infty$  at the end of the calculation. Thus,  $N_k$  is determined from the condition

$$1 = \int_0^L dz |\psi_k(z)|^2 . \quad (69)$$

To do the normalization integral, we utilize the fact that in the limit  $L \rightarrow \infty$  the contribution to the integral coming from small  $z$  is negligibly small compared to the contribution coming from large  $z$ . Hence, we can replace in (69)  $\psi_k(z)$  by its asymptotic form for large  $z$ :

$$\psi_k(z) \sim \psi_k^{\text{in}}(z) + \psi_k^{\text{out}}(z) \quad (70)$$

$$= N_k \left[ \frac{\exp[-\pi/2k]}{\Gamma(1+ik^{-1})} \exp[ikx/4] + \frac{\exp[-\pi/2k + i\pi]}{\Gamma(1-ik^{-1})} \exp[-ikx/4] \right] , \quad (71)$$

where we defined in- and outgoing waves which we need in appendix B for the calculation of  $s_e$ .

The normalization constant is then given by

$$N_k = \sqrt{\frac{\pi}{Lk(1 - \exp[-2\pi/k])}} = \frac{\mathcal{N}_k}{\sqrt{L}} \quad (72)$$

which also defines  $\mathcal{N}_k$  needed in appendix B.

Having appropriately normalized wavefunctions, we can now calculate the electronic matrix element (41). Although we could calculate (41) for any  $\mathbf{R}$  and any  $k$  we give only the result for  $\mathbf{R} = 0$  and  $k \ll 1$  because in the calculation of  $s_e$  and  $\tau_e$  we eventually approximate (41) by  $I_{nk \ll 1}^{(1)}(0)$ . The multidimensional integrals defining  $s_e$  and  $\tau_e$  are then easier to perform.

The matrix element we need is

$$I_{nk}^{(1)}(0) = 2n\mathcal{N}_n\mathcal{N}_k \int_0^\infty dy \exp[-y/d] W_{n,1/2}(y) M_{-ik^{-1},1/2}(ikny) . \quad (73)$$

Approximating  $\mathcal{N}_k \approx (\pi/k)^{1/2}$  for  $k \ll 1$  gives

$$I_{nk \ll 1}^{(1)}(0) = \sqrt{\frac{\pi}{nk}} \frac{1}{\Gamma(n)} I_1 \quad (74)$$

with

$$I_1 = \int_0^\infty dy \exp[-y/d] W_{n,1/2}(y) M_{-ik^{-1},1/2}(ikny) , \quad (75)$$

which, to be consistent, we also have to calculate for  $k \ll 1$ .

To determine the integral  $I_1$ , we use the expansion (64) for  $W_{n,1/2}(y)$  together with the expansion [74]

$$M_{-ik^{-1},1/2}(ikny) = ikn \sum_{m=0}^{\infty} C_m \frac{(ikn)^m}{[n(1-ik)]^{(m+1)/2}} y^{(m+1)/2} J_{m+1}(2\sqrt{ny(1-ik)}) \quad (76)$$

for  $M_{-ik^{-1},1/2}(ikny)$ , where  $C_m$  are constants and  $J_n(y)$  are Bessel functions<sup>1</sup>. Thus,

$$I_1 = ikn \sum_{m=0}^{\infty} \sum_{q=0}^n a_q C_m \frac{(ikn)^m}{[n(1-ik)]^{(m+1)/2}} I_2 \quad (77)$$

with an integral  $I_2$  which can be found in [75]:

$$\begin{aligned} I_2 &= \int_0^\infty dy \exp[-(1/d + 1/2)y] \exp[n - q + (m+1)/2] J_{m+1}(2\sqrt{ny(1-ik)}) \\ &= \left(\frac{2d}{2+d}\right)^{n-q+m+2} (n-q)![(1-ik)n]^{(m+1)/2} \exp\left[-(1-ik)\frac{2nd}{2+d}\right] L_{n-q}^{(m+1)}((1-ik)\frac{2nd}{2+d}) \end{aligned} \quad (78)$$

with  $d = 1/2nk_s$ .

Inserting (78) for  $k \ll 1$  into (77) and using  $C_0 = 1$  we finally obtain

$$|I_{nk \ll 1}^{(1)}(0)|^2 = k |I_n^{(1)}|^2 = \pi nk \left(\frac{2d}{2+d}\right)^4 |f_n|^2 \quad (79)$$

with

$$|f_n|^2 = \sum_{q=0}^n \frac{(-)^q}{q!} \frac{\Gamma(n+1)}{\Gamma(n-q)} \left(\frac{2d}{2+d}\right)^{n-q} \exp\left[-\frac{2nd}{2+d}\right] L_{n-q}^{(1)}\left(\frac{2nd}{2+d}\right) , \quad (80)$$

where Eq. (79) defines  $|I_n^{(1)}|^2$  used in appendix B.

<sup>1</sup> Specifically, we employ formula 13.3.8 from [74] with  $h = 1/2$ .

Finally we give the result for the matrix element (42) for  $\mathbf{R} = 0$ . Using the single electron states of the metal specified in (37) and measuring length again in units of  $a_B$ ,

$$I_{kk'}^{(2)}(0) = 2 \int_0^\infty dx \exp[-k_s x] \sin(kx) \sin(k'x) \quad (81)$$

$$= 16k_s^2 \frac{\sqrt{E_k E_{k'}}}{[(k_s^2 + E_k + E_{k'})^2 - 4E_k E_{k'}]^2} k k' \quad (82)$$

$$= 16k_s^2 J^{(2)}(E_k, E_{k'}) k k' , \quad (83)$$

which also defines the function  $J^{(2)}(E_k, E_{k'})$ , with  $E_k = k^2$  and likewise for  $E_{k'}$ , needed in appendix B.

## B Calculation of $s_e$ and $\tau_e$

In this appendix we give mathematical details concerning the calculation of  $s_e$  and  $\tau_e$ . In all equations below we use dimensionless variables measuring energies and lengths in units of  $R_0$  and  $a_B$ , respectively. We are furthermore interested in the limit  $L \rightarrow \infty$  and  $A \rightarrow \infty$ . Thus, momentum sums become integrals according to

$$\frac{1}{L} \sum_k = \int \frac{dk}{2\pi} \quad \text{and} \quad \frac{1}{A} \sum_{\mathbf{Q}} = \int \frac{d\mathbf{Q}}{(2\pi)^2} . \quad (84)$$

For the purpose of doing some of the integrals analytically, we found it convenient to rewrite the  $\delta$ -function for energy conservation as follows:

$$\delta(E_{\mathbf{Q}'q'} - E_{\mathbf{Q}n} + E_{\mathbf{K}'k'} - E_{\mathbf{K}k}) = \int_{-\infty}^{\infty} d\omega \delta(E_{\mathbf{Q}'q'} - E_{\mathbf{Q}n} - \omega) \delta(E_{\mathbf{K}'k'} - E_{\mathbf{K}k} + \omega) . \quad (85)$$

The angles can then be integrated out and the global sticking coefficient  $s_e$  defined in Eq. (49) becomes

$$s_e = \frac{4\beta_e^{3/2}}{\pi^2 \beta_s^{1/2}} \sum_n \int_0^\infty dq' \int_0^\infty dk \int_0^\infty dk' \int_{-\infty}^\infty d\omega \int_0^\infty dR \frac{|I_{nq'}^{(1)}(0) I_{kk'}^{(2)}(0)|^2}{k_s^2 + R^2} \times [1 + n_B(\omega)] N(R, \omega, E_k, E_{k'}) R^{-1} \exp[-\beta_e \Psi_n(R, \omega, E_{q'})] , \quad (86)$$

where, for simplicity, we have neglect the dependence of the electronic matrix elements (41) and (42) on the lateral momentum transfer  $\mathbf{R} = \mathbf{Q} - \mathbf{Q}'$  and introduced two functions:

$$N(R, \omega, E_k, E_{k'}) = F_{-1/2}(\beta_s(E_F - y_{kk'}(R, \omega) + \omega) - F_{-1/2}(\beta_s(E_F - y_{kk'}(R, \omega))) , \quad (87)$$

$$\Psi_n(R, \omega, E_{q'}) = E_n + \omega + \left( \frac{E_{q'} - E_n + R^2 - \omega}{2R} \right)^2 , \quad (88)$$

with  $F_{-1/2}(x)$  Fermi integrals for which, as far as the numerics is concerned, we take Unger's approximation [76], and

$$y_{kk'}(R, \omega) = E_k + \left( \frac{E_k - E_{k'} - R^2 - \omega}{2R} \right)^2 \quad (89)$$

with  $E_k = k^2$  and likewise for  $E_k$  and  $E_{q'}$ . The functions  $I_{nq'}^{(1)}(0)$  and  $I_{kk'}^{(2)}(0)$  are, respectively, defined in Eqs. (73) and (81) in appendix A.

Using  $E_{q'}$ ,  $E_k$ , and  $E_{k'}$  instead of  $q'$ ,  $k$ , and  $k'$  as integration variables, we finally find the result presented in Eqs. (50) and (51) with

$$h(R, \omega) = \sum_n |I_n^{(1)}|^2 \exp[-\beta_e(E_n + \omega)] \int_{x_n(R, \omega)}^\infty dx \exp[-\beta_e x^2] , \quad (90)$$

$$g(R, \omega) = \int_0^\infty dE dE' J^{(2)}(E, E') N(R, \omega, E, E') , \quad (91)$$

and

$$x_n(R, \omega) = \frac{R^2 - E_n - \omega}{2R} . \quad (92)$$

The calculation of the energy resolved sticking coefficient proceeds along the same lines. For perpendicular incidence we find the result stated in Eq. (52) of the main text with

$$g^\perp(R, E') = \sum_n |I_n^{(1)}|^2 \frac{1 + n_B(E' - E_n - R^2)}{1 + (R/k_s)^2} g(R, E' - E_n - R^2) . \quad (93)$$

Now we turn our attention to the calculation of the desorption time. It is quite similar. An intermediate expression, after expressing energy conservation in the form (85) and performing the integrals over angles, is

$$\begin{aligned} \tau_e^{-1} = & \frac{R_0}{8\pi^3 \hbar Z} \sum_{n'} \int_0^\infty dq \int_0^\infty dk \int_0^\infty dk' \int_{-\infty}^\infty d\omega \int_0^\infty dR \frac{|I_{qn'}^{(1)}(0)I_{kk'}^{(2)}(0)|^2}{k_s^2 + R^2} \\ & \times [1 + n_B(\omega)] N(R, \omega, E_k, E_{k'}) R^{-1} \exp[-\beta_s \Phi_{n'}(R, \omega, E_q)] , \end{aligned} \quad (94)$$

where we have again neglected the dependence of the electronic matrix elements (41) and (42) on the transfer of lateral momentum and introduced

$$Z = \sum_n \exp[-\beta_s E_n] , \quad (95)$$

$$\Phi_{n'}(R, \omega, E_q) = E_q + \omega + \left( \frac{E_q - E_{n'} - R^2 + \omega}{2R} \right)^2 . \quad (96)$$

Using again  $E_k = k^2$ ,  $E_{k'} = k'^2$ , and  $E_q = q^2$  as integration variables we finally find the result (56) and (57) given in main text with

$$f(R, \omega) = \sum_n |I_n^{(1)}|^2 \exp[-\beta_e E_n] \int_{y_n(R, \omega)}^\infty dy \exp[-\beta_s y^2] \quad (97)$$

and

$$y_n(R, \omega) = \frac{\omega + R^2 - E_n}{2R} . \quad (98)$$

At the end of this appendix let us say a few words about Laplace's approximation [77] which we used to derive Eqs. (59)–(61). If there is only a single bound state with energy  $E_1$  the summations over  $n$  reduce to a single term. For  $kT_s \ll |E_1|$  and  $kT_e \ll |E_1|$  it is then possible to do some of the integrals defining  $s_e$  and  $\tau_e$  asymptotically within Laplace's approximation.

First, we consider Laplace's approximation for  $\tau_e$ . For a single bound state

$$f(R, \omega) = |I_1^{(1)}|^2 \exp[-\beta_e E_1] \int_{y_1(R, \omega)}^\infty dy \exp[-\beta_s y^2] . \quad (99)$$

Provided  $kT_s \ll |E_1|$ ,  $f(R, \omega)$  is largest for  $y_1(R, \omega) \leq 0$ , that is, for  $\omega \leq E_1 - R^2 < 0$ . In this domain, Laplace's approximation to the  $y$ -integral gives  $\sqrt{\pi/\beta_s}/2$ , where the factor 1/2 anticipates that the  $R$ - and  $\omega$ -integrations are later performed also within Laplace's approximation. Changing  $\omega \rightarrow -\omega$ , we obtain

$$I_{\text{desorb}}^L \approx \frac{1}{2} \frac{\pi^{1/2}}{\beta_s^{1/2}} \int_0^\infty dR \int_{|E_1|+R^2}^\infty d\omega \frac{n_B(\omega)}{1 + (R/k_s)^2} |I_1^{(1)}|^2 \exp[-\beta_e E_1] [-g(R, -\omega)] , \quad (100)$$

where we used  $1 + n_B(-\omega) = -n_B(\omega)$ . Hence, using (56)

$$\tau_e^L \approx \frac{4\pi^{5/2} \beta_s^{1/2} \hbar}{R_0 |I_1^{(1)}|^2 J(|E_1|)} , \quad (101)$$

where

$$J(|E_1|) = \int_0^\infty dR \int_{|E_1|+R^2}^\infty d\omega \frac{n_B(\omega)}{1 + (R/k_s)^2} [-g(R, -\omega)] . \quad (102)$$

Since  $kT_s \ll |E_1|$ , we can approximate in Eq. (102) the Bose distribution function  $n_B(\omega)$  by  $\exp[-\beta_s \omega]$ . Hence, the main contribution to the  $\omega$ -integral will come from its lower boundary. Calculating the  $\omega$ -integral within Laplace's approximation and then applying, in a last step, Laplace's approximation also to the remaining  $R$ -integral, we find

$$J(|E_1|) \approx \frac{\pi^{1/2}}{2\beta_s^{3/2}} \bar{g} \exp[-\beta_s |E_1|] \quad (103)$$

with

$$\bar{g} = \lim_{R \rightarrow 0} [-g(R, -|E_1|)] , \quad (104)$$

which, combined with Eq. (101), leads to Eq. (60) given in the main text.

Calculating  $s_e$  within Laplace's approximation is quite similar. However, whereas for  $\tau_e$  it is a reasonable approximation, because  $kT_s \ll |E_1|$ , for  $s_e$  it is only meaningful when  $kT_e$  is also much smaller than  $|E_1|$ . Under this assumption, which is of course usually not satisfied, we find from Eq. (51), again anticipating that the  $R$ - and  $\omega$ -integrations are later performed within Laplace's approximation,

$$I_{\text{stick}}^L \approx \frac{1}{2} \frac{\pi^{1/2}}{\beta_e^{1/2}} |I_1^{(1)}|^2 \exp[\beta_e |E_1|] K(|E_1|) \quad (105)$$

with

$$K(|E_1|) = \int_0^\infty dR \int_{|E_1|+R^2}^\infty d\omega \frac{1+n_B(\omega)}{1+(R/k_s)^2} \exp[-\beta_e \omega] g(R, \omega) , \quad (106)$$

to which we again successively apply Laplace's approximation to find

$$K(|E_1|) \approx \frac{\pi^{1/2}}{2\beta_e^{3/2}} \tilde{g} \exp[-\beta_e |E_1|] \quad (107)$$

with

$$\tilde{g} = \lim_{R \rightarrow 0} [g(R, |E_1|)] . \quad (108)$$

Hence, combining (107) and (105) and inserting the result in (50) gives

$$s_e^L = \frac{4|I_1^{(1)}|^2 \tilde{g}}{\pi \beta_s^{1/2} \beta_e^{1/2}} . \quad (109)$$

Using the properties of the function  $g(R, \omega)$  we now show that  $\tilde{g} = \bar{g}$ . First, we see from the definition (91) that the  $R$ -dependence of  $g(R, |E_1|)$  comes from the  $R$ -dependence of the function  $y_{kk'}(R, |E_1|)$  defined in (89). Then we notice that

$$\lim_{R \rightarrow 0} y_{kk'}(R, |E_1|) = \begin{cases} \infty & \text{for } E \neq E' + |E_1| \\ E & \text{for } E = E' + |E_1| \end{cases} , \quad (110)$$

from which follows

$$\lim_{R \rightarrow 0} N(R, |E_1|, E, E') = \begin{cases} 0 & \text{for } E \neq E' + |E_1| \\ F_{-1/2}(\beta_s(E_F - E + |E_1|)) - F_{-1/2}(\beta_s(E_F - E)) & \text{for } E = E' + |E_1| \end{cases} , \quad (111)$$

because  $F_{-1/2}(x)$  vanishes for  $x \rightarrow -\infty$ , and thus

$$\tilde{g} = \lim_{R \rightarrow 0} g(R, |E_1|) \quad (112)$$

$$= \int_0^\infty dE' J^{(2)}(E' + |E_1|, E') [F_{-1/2}(\beta_s(E_F - E')) - F_{-1/2}(\beta_s(E_F - E' - |E_1|))] \quad (113)$$

$$= \int_0^\infty dE' J^{(2)}(E', E' + |E_1|) [F_{-1/2}(\beta_s(E_F - E')) - F_{-1/2}(\beta_s(E_F - E' - |E_1|))] , \quad (114)$$

where in the last line we used  $J^{(2)}(E, E') = J^{(2)}(E', E)$ . To calculate  $\bar{g}$  we proceed in the same way, noticing however that  $N(R, -|E_1|, E, E')$  is finite only for  $E' = E + |E_1|$ . Hence,

$$\bar{g} = \lim_{R \rightarrow 0} [-g(R, -|E_1|)] \quad (115)$$

$$= - \int_0^\infty dE J^{(2)}(E, E + |E_1|) [F_{-1/2}(\beta_s(E_F - E - |E_1|)) - F_{-1/2}(\beta_s(E_F - E))] \quad (116)$$

$$= \int_0^\infty dE J^{(2)}(E, E + |E_1|) [F_{-1/2}(\beta_s(E_F - E)) - F_{-1/2}(\beta_s(E_F - E - |E_1|))] \quad (117)$$

$$= \tilde{g} . \quad (118)$$

Since  $\tilde{g} = \bar{g}$ , Eq. (109) is identical to Eq. (59) given in the main text.

Support from the SFB-TR 24 “Complex Plasmas” and discussions with H. Kersten are greatly acknowledged.

## References

1. R. N. Franklin, *J. Phys. D: Appl. Phys.* **36** (2006) R309.
2. K.-U. Riemann, *J. Phys. D: Appl. Phys.* **24** (1991) 493.
3. H. G. Purwins, *Plasma* **2007** **993** (2008) 67.
4. H. G. Purwins, H. U. Bodeker, A. W. Liehr, *Experimental Chaos* **742** (2004) 289.
5. M. A. Lieberman, A. J. Lichtenberg, *Principles of plasma discharges and materials processing* (Wiley-Interscience, New York) (2005).
6. M. W. Cole, *Rev. Mod. Phys.* **46** (1974) 451.
7. T. Ando, A. B. Fowler, F. Stern, *Rev. Mod. Phys.* **54** (1982) 437.
8. M. Rapp, F.-J. Luebken, *J. Atmospheric and solar-terrestrial physics* **63** (2001) 759.
9. H. B. Garrett, A. C. Whittlesey, *IEEE transactions on plasma science* **28** (2000) 2017.
10. E. C. Whipple, *Rep. Prog. Phys.* **44** (1981) 1197.
11. I. Mann, *Advances in Space Research* **41** (2008) 160.
12. M. Horányi, *Annu. Rev. Astron. Astrophys.* **34** (1996) 383.
13. O. Ishihara, *J. Phys. D: Appl. Phys.* **40** (2007) R121.
14. V. E. Fortov, A. V. Ivlev, S. A. Khrapak, A. G. Khrapak, G. E. Morfill, *Phys. Rep.* **421** (2005) 1.
15. S. A. Khrapak, S. V. Ratynskaia, A. V. Zobnin, A. D. Usachev, V. V. Yaroshenko, M. H. Thoma, M. Kretschmer, H. Hoefner, G. E. Morfill, O. F. Petrov, V. E. Fortov, *Phys. Rev. E* **72** (2005) 016406.
16. A. A. Samarian, S. V. Vladimirov, *Phys. Rev. E* **67** (2003) 066404.
17. E. B. Tomme, B. M. Annaratone, J. E. Allen, *Plasma Sources Sci. Technol.* **9** (2000) 87.
18. E. B. Tomme, D. A. Law, B. M. Annaratone, J. E. Allen, *Phys. Rev. Lett.* **85** (2000) 2518.
19. B. Walch, M. Horányi, S. Robertson, *Phys. Rev. Lett.* **75** (1995) 838.
20. M. Li, C. Li, H. Zhan, J. Xu, *Appl. Phys. Lett.* **92** (2008) 031503.
21. L. Stollenwerk, J. G. Laven, H.-G. Purwins, *Phys. Rev. Lett.* **98** (2007) 255001.
22. L. Stollenwerk, S. Amiranashvili, J.-P. Boeuf, H.-G. Purwins, *Phys. Rev. Lett.* **96** (2006) 255001.
23. M. Li, C. Li, H. Zhan, J. Xu, *Proceedings of the XV International Conference on Gas Discharges and their Applications* (2004).
24. U. Kogelschatz, *Plasma Chemistry and Plasma Processing* **23** (2003) 1.
25. Y. B. Golubovskii, V. A. Maiorov, J. Behnke, J. F. Behnke, *J. Phys. D: Appl. Phys.* **35** (2002) 751.
26. K. G. Emeleus, J. R. M. Coulter, *Int. J. Electronics* **62** (1987) 225.
27. J. F. Behnke, T. Bindemann, H. Deutsch, K. Becker, *Contrib. Plasma Phys.* **37** (1997) 345.
28. H. Kersten, H. Deutsch, G. M. W. Kroesen, *Int. J. Mass Spectrometry* **233** (2004) 51.
29. F. X. Bronold, H. Fehske, H. Kersten, H. Deutsch, *Phys. Rev. Lett.* **101** (2008) 175002.
30. J. E. Lennard-Jones, A. F. Devonshire, *Proc. Roy. Soc. (London) A* **156** (1936) 6.
31. B. Bendow, S.-C. Ying, *Phys. Rev. B* **7** (1973) 622.
32. Z. W. Gortel, H. J. Kreuzer, R. Teshima, *Phys. Rev. B* **22** (1980) 5655.
33. Z. W. Gortel, H. J. Kreuzer, R. Teshima, *Phys. Rev. B* **22** (1980) 512.
34. W. Brenig, *Z. Phys. B* **48** (1982) 127.
35. H. J. Kreuzer, Z. W. Gortel, *Physisorption Kinetics* (Springer Verlag, Berlin) (1986).
36. D. Neilson, R. M. Nieminen, J. Szymański, *Phys. Rev. B* **33** (1986) 1567.
37. Z. W. Gortel, J. Szymanski, *Phys. Rev. B* **43** (1991) 1919.
38. W. Brenig, R. Russ, *Surface Science* **278** (1992) 397.
39. A. B. Walker, K. O. Jensen, J. Szymański, D. Neilson, *Phys. Rev. B* **46** (1992) 1687.
40. E. Evans, D. L. Mills, *Phys. Rev. B* **8** (1973) 4004.
41. G. Barton, *J. Phys. C: Solid State Phys.* **14** (1981) 3975.
42. V. Dose, W. Altmann, A. Goldmann, U. Kolac, J. Rogozik, *Phys. Rev. Lett.* **52** (1984) 1919.
43. D. Straub, F. J. Himpsel, *Phys. Rev. Lett.* **52** (1984) 1922.
44. D. P. Woodruff, S. L. Hulbert, P. D. Johnson, N. V. Smith, *Phys. Rev. B* **31** (1985) (RC)4046.
45. P. M. Echenique, J. B. Pendry, *Progr. Surface science* **32** (1990) 111.
46. A. Elmahboubi, Y. Lépine, *Surface science* **303** (1994) 409.
47. T. Fauster, *Appl. Phys. A* **59** (1994) 479.
48. A. Elmahboubi, Y. Lépine, *Solid State Commun.* **94** (1995) 655.
49. U. Höfer, I. L. Shumay, C. Reuss, U. Thomann, W. Wallauer, T. Fauster, *Science* **277** (1997) 1480.
50. E. V. Chulkov, V. M. Silkin, P. M. Echenique, *Surface science* **437** (1999) 330.
51. U. Höfer, *Appl. Phys. B* **68** (1999) 383.
52. M. Lampe, V. Gavriishchaka, G. Ganguli, G. Joyce, *Phys. Rev. Lett.* **86** (2001) 5278.
53. M. Lampe, R. Goswami, Z. Sternovsky, S. Robertson, V. Gavriishchaka, G. Ganguli, G. Joyce, *Phys. Plasma* **10** (2003) 1500.
54. Z. Sternovsky, M. Lampe, S. Robertson, *IEEE Trans. Plasma Science* **32** (2004) 632.
55. I. B. Bernstein, I. N. Rabinowitz, *Phys. Fluids* **2** (1959) 112.
56. J. G. Laframboise, L. W. Parker, *Phys. Fluids* **16** (1973) 629.
57. J. E. Daugherty, R. K. Porteous, M. D. Kilgore, D. B. Graves, *J. Appl. Phys.* **72** (1992) 3934.
58. D. D. Tskhakaya, N. L. Tsintsadze, P. K. Shukla, L. Stenflo, *Phys. Scripta* **64** (2001) 366.
59. D. D. Tskhakaya, P. K. Shukla, L. Stenflo, *Phys. Plasmas* **8** (2001) 5333.
60. C. J. F. Boettcher, *Theory of electric polarization* (Elsevier Publishing Company, Amsterdam) (1952).
61. B. T. Draine, B. Sutin, *The Astrophysical Journal* **320** (1987) 803.
62. Y. M. Vilk, A. E. Ruckenstein, *Phys. Rev. B* **48** (1993) 11196.
63. M. J. Richardson, *Phys. Rev. A* **8** (1973) 781.
64. V. C. Liu, *Space Science Reviews* **9** (1969) 423.
65. G. H. P. M. Swinkels, H. Kersten, H. Deutsch, G. M. W. Kroesen, *J. Appl. Phys.* **88** (2000) 1747.
66. S. J. Choi, M. J. Kushner, *IEEE Trans. Plasma Science* **22** (1994) 138.
67. H. Mauer, R. Basner, H. Kersten, *Rev. Sci. Instrum.* **79** (2008) 093508.

68. J. Maultsch, S. Reich, C. Thomsen, H. Requardt, P. Ordejón, *Phys. Rev. Lett.* **92** (2004) 075501.
69. N. W. Ashcroft, N. D. Mermin, *Solid State Physics* (Holt, Rinehart and Winston, New York) (1976).
70. I. Kuscer, *Surf. Sci.* **25** (1971) 225.
71. T. Umebayashi, T. Nakano, *Publ. Astron. Soc. Japan* **32** (1980) 405.
72. D. Hollenbach, E. E. Salpeter, *J. Chem. Phys.* **53** (1970) 79.
73. M.-C. Desjonquieres, D. Spanjaard, *Concepts of surface physics* (Springer Verlag, Berlin) (1996).
74. M. Abramowitz, I. A. Stegun, editors, *Handbook of mathematical functions* (Dover Publications, Inc., New York) (1973).
75. I. S. Gradshteyn, I. M. Ryzhik, *Tables of series, products, and integrals*, Vol. 2 (Verlag Harri Deutsch, Thun and Frankfurt/Main) (1981).
76. K. Unger, *sol. stat. phys. (b)* **149** (1988) K141.
77. F. W. J. Olver, *Asymptotics and special functions* (Academic Press, New York) (1974).